Available online at www.sciencedirect.com
ScienceDirect
International Journal of Mass Spectrometry 255–256 (2006) 312–327
International Journal of Mass Spectrometry
www.elsevier.com/locate/ijms

Gas-phase ion–molecule reactions for resolution of atomic isobars: AMS and ICP-MS perspectives

Dmitry R. Bandura [a,*], Vladimir I. Baranov [a], A.E. Litherland [b], Scott D. Tanner [a]

[a] University of Toronto, Institute of Biomaterials and Biomedical Engineering, 164 College Street, Toronto, Ontario, Canada M5S 3G9
[b] University of Toronto, IsoTrace Laboratory, 60 St. George Street, Toronto, Ontario, Canada M5S 1A7

Received 2 March 2006; received in revised form 20 June 2006; accepted 21 June 2006
Available online 1 August 2006

This paper is dedicated to Prof. Diethard Kurt Bohme on the occasions of his 65th birthday.

Abstract

Ion–molecule reactions that can be used for resolution of spectral overlaps of long-lived or stable ($T_{1/2} > 100$ years) atomic isobars on the long-lived radio-isotopes ($100 < T_{1/2} < 10^{12}$ years) in mass spectrometry are considered. Results for the separations of isobaric overlaps via cation reactions with NO, N_2O, O_2, CO_2, C_2H_2, CH_3F studied with the Inductively Coupled Plasma Dynamic Reaction Cell™ Mass Spectrometer (ICP-DRC™-MS) with use of stable isotopes are presented. Overview of potential and reported reactions for separation of 35 isobars is given. Potential for the following isobaric pairs separation is shown (reaction gas and the extent of separation achieved to date in parenthesis): $^{32}Si^+/^{32}S^+$(NO, 5×10^4), $^{40}K^+/^{40}Ar^+$(N_2O, 1.9×10^3), $^{40}K^+/^{40}Ca^+$(N_2O, 50), $^{59}Ni^+/^{59}Co^+$(N_2O, 6), $^{79}Se^+/^{79}Br^+$(O_2, 7.2×10^3), $^{81}Kr^+/^{81}Br^+$(C_2H_2, 1.5×10^4), $^{93}Mo^+/^{93}Nb^+$(N_2O, 100), $^{93}Mo^+/^{93}Zr^+$(N_2O, 150), $^{135}Cs^+/^{135}Ba^+$(N_2O, 8×10^4), $^{137,138}La^+/^{137,138}Ba^+$($O_2$, 40), $^{146}Sm^+/^{146}Nd^+$(CO_2, 1.5×10^5), $^{176}Lu^+/^{176}Hf^+$(NO, 2.8×10^3), $^{187}Re^+/^{187}Os^+$(N_2O, 2.8×10^4). Effect of instrumental parameters on reactivity is discussed. The relevance of this work to accelerator mass spectrometry is discussed briefly.

Keywords: Atomic isobars; Gas-phase ion–molecule reactions; Chemical resolution; Dynamic reaction cell; Accelerator mass spectrometry; Inductively coupled plasma mass spectrometry

1. Introduction

The separation of isobaric overlaps is of great importance to mass spectrometry, whether they are stable isotopes such as ^{40}Ar and ^{40}Ca, very long-lived radioactive isotopes like ^{187}Re and stable ^{187}Os or radioactive isotopes like ^{14}C. In the latter case the radiocarbon isotope, which ranges naturally from an isotope ratio of $^{14}C/^{12}C$ of 10^{-12} to below 10^{-18}, is extremely rare compared with ^{14}N. These isobars in natural samples are not resolvable by mass measurements alone because they are so close in mass like Re/Os, where $M/\Delta M \sim 6.2 \times 10^7$, or so different in relative intensity like $^{14}C/^{12}C$. As a result they must be separated by some physical or chemical method.

The attenuation of the unwanted isobar required in various cases is quite different. In general, the extent of separation required will be higher for rare radioactive atoms than for rare stable atoms. The natural $^{187}Re/^{187}Os$ ratio can be near 3 and so an attenuation of 1000 of, for example the ^{187}Re isobar, can lead to adequate measurements of $^{187}Os/Os$. In the case of ^{14}C the natural ratio of $^{14}C/C$ is near 10^{-12} and so an attenuation of the abundant isobar ^{14}N and the abundant molecules ^{13}CH and $^{12}CH_2$ of at least 10^8 is needed. In the second case some variant of accelerator mass spectrometry (AMS) [1] can be employed. The large natural ratio completely prevents separation, in this case, by mass resolution in a mass spectrometer.

The remarkable attenuation observed in ammonia gas of 10^8 for the eV $^{40}Ar^+$ ions, with the $^{40}Ca^+$ ions affected very little [12], was an early indication of the possible great importance of the reaction cell technology to isobars separation, first shown in ICP-MS by Douglas [2] and Rowan and Houk [3]. The exponential decay of the Ar^+ with gas pressure over so many decades and the very low level of loss of the accompanying Ca^+ ions are due to two remarkable features of the rf-quadrupole based reaction cell [4]. First, trapping of ions in the potential

* Corresponding author. Tel.: +1 416 946 8420; fax: +1 416 978 4317.
E-mail address: dmitry.bandura@utoronto.ca (D.R. Bandura).

1387-3806/$ – see front matter © 2006 Elsevier B.V. All rights reserved.
doi:10.1016/j.ijms.2006.06.012

well of rf-field enables conditions under which multiple collisions do not cause significant scattering loss of a wanted isobar and can even focus ions close to the axis through collisional focusing [5]. Second, for low (<eV) ion energy, the reaction gas can be specifically selected to be reactive only towards the unwanted isobar. As a result, the extent of the unwanted isobar suppression, which is exponential with the number of reactive collisions, can be extremely high. In commercial ICP-MS instruments, ion–molecular reactors are implemented as rf powered multipoles. Rf-only octopole [6], hexapole[7,8] and rf-dc quadrupole [9–11] are used, with the latter (Dynamic Reaction Cell^{TM}, DRC) operated in a mass-bandpass mode that prevents in-cell formation of new polyatomic ions [12]. The prevention of formation of unwanted new polyatomic ions at correct mass-bandpass selection enables use of high reactivity gases [13]. The mass bandpass operation is based on the ion stability characteristics of the quadrupole field. At given rf frequency, amplitude and resolving dc voltage, stability of an ion in the quadrupole field depends only on its mass-to-charge ratio, m/z (unlike in higher order multipoles, where it also depends on the ion coordinate [14]). As a result, if the mass bandpass is selected such that precursors of unwanted product ions have m/z that fall outside the selected mass band, the precursors are quickly (within 1–2 rf cycles) ejected from the field and the unwanted reactions are barred. For an ion–molecule reactor preceding AMS, bandpass operation may be less critical since the new polyatomic ions will be destroyed in the stripping canal of AMS.

When a relatively heavy gas is used, the scattering losses are countered by the addition of a small electric field along the axis of the quadrupole [15]. This can be large enough to keep the ions moving in the same direction in spite of the cooling tendency of the elastic collisions and the angular scattering, yet small enough not to affect the kinetic energy to the extent of promoting highly endothermic processes [16].

Isobaric interferences that are relevant to routine ICP-MS analysis are mainly polyatomic, since there is little overlap between major isotopes of most elements analysed by ICP-MS ($^{40}Ca^+/^{40}Ar^+$ overlap being an important exception). The most abundant interferences usually contain plasma- and/or sample matrix elements, for example, argon (Ar^+ and ArX^+, where X = Ar, O, Cl, C, N, H, etc.). Electron transfer reactions with ammonia in the DRC efficiently neutralise CN^+, CNH^+, ArH^+, Ar^+, ClO^+, ArC^+, $ClOH^+$, $ArOH^+$ and ArO^+ interferences on Al^+, K^+, Ca^+, V^+, Cr^+, Mn^+ and Fe^+, respectively [11], without significant loss of the analyte ions. Other gases (methane, oxygen, hydrogen) are successfully used in cell-based ICP-MS to enable electron, hydrogen atom-, proton- and oxygen atom-transfer for the suppression of common spectral overlaps [17,18].

Another approach to address the issue of spectral interferences is to use high-resolution mass analyzers. Modern magnetic sector ICP-MS provide resolving power in excess of $R_{10\%} = 10{,}000$ [19,20] which allows resolution of many polyatomic interferences. Despite successes in development of high mass resolving power analyzers [21,22] it is obvious that even FT-ICR-MS cannot resolve many atomic isobaric overlaps, especially if the abundance of an overlapping isobar is much higher than that of an analyte (see Table 1 for $M/\Delta M$ values required).

Using ICP-MS, Rowan and Houk have shown that Ar^+ can be reacted in charge exchange with xenon, allowing detection of non-reactive isobaric atomic $^{40}Ca^+$[3]. The potential of ion–molecule reactions for the resolution of isobaric atomic interferences in ICP-MS was further recognised and demonstrated by Eiden et al. [23], who have shown that reactions with O_2 can potentially be applied to the detection of $^{90}Sr^+$ in the presence of $^{90}Zr^+$ and $^{90}Y^+$, and $^{129}I^+$ in the presence of $^{129}Xe^+$. Oxidation, hydroxylation and chlorination of Sr^+ with N_2O, $N_2O + CH_4$ and CH_3Cl, respectively was demonstrated for resolution of the $^{87}Rb^+/^{87}Sr^+$ overlap [13]. Fluorination with CH_3F and detection of Sr as SrF^+ was used for Rb/Sr age determination of magmatic rocks [24]. Recently, Tanner et al. reported on resolution of $^{238}Pu^+/^{238}U^+$ and $^{238}Pu^+/^{238}UH^+$ in reaction with CO_2 and Am^+/Pu^+ in reactions with NO enabled in ICP-DRC-MS [25].

ICP-MS as a method of detection of radio-isotopes can theoretically be advantageous for relatively long-lived isotopes (half-life $T_{1/2} > 10^2$ years) [26]. In practice, spectral overlaps limit ICP-MS capabilities. Table 1 lists isotopes with $100 < T_{1/2} < 10^{12}$ years which have long-lived ($T_{1/2} > 100$ years) or stable atomic isobars. Use of ion–molecule reactions for resolving atomic isobaric overlaps can potentially provide means to utilise the high sensitivity of current ICP-MS for radio nuclide detection. Two major approaches to such separations were discussed previously [13], and have recently been considered in detail by Olesik and Jones [17]. The more preferable approach is to remove an interfering ion by a relatively fast reaction with a neutral which has no or very low reactivity towards an analyte ion. The alternate approach is to form an analyte-containing product ion at a different, less interfered m/z. In some cases, when both isobars need to be measured, the only way to do it simultaneously is to move one or another isobar to a different m/z via its complete conversion to a product ion(s). When AMS is considered, simultaneous elimination of the isobar and formation of an analyte containing molecular ion may be desirable: conversion of molecular cations to anions for tandem accelerator can in many cases be accomplished easier, due to the generally higher electron affinity of molecules compared to atoms.

Data on the reactivity of atomic cations with many molecules are available in the literature. Reaction rate constants have been measured by a variety of methods and are most comprehensively compiled in the recent publication by Anicich [27], which cites over 2300 original papers published over 50 years (up to 2003). Most reaction rate constants were obtained by ion cyclotron resonance (ICR), selected ion flow tube (SIFT), drift tube (DT) and guided ion beam (GIB) experiments. Over the last 5 years comprehensive studies of reaction kinetics of many ICP-produced singly charged cations with gases potentially useful in ICP-MS (due to their relatively low molecular weight), including N_2O [28,29], O_2 [29,30], NO [31], CO_2 [32], CH_3F [33], were conducted in D.K. Bohme's laboratory using the ICP-SIFT [34,35]. Unpublished data on ICP-produced cations reactivity towards NH_3, CH_4 and H_2O are available from the laboratory's website [36]. The reaction kinetics data provide an important basis for

Table 1
Isobaric atomic overlaps for radio-isotopes with $100 < T_{1/2} < 10^{12}$ years and ion–molecule chemistries for their post-ionisation separation

m/z	Radio-isotope	$T_{1/2}$ (years)	Isobar	M/ΔM	Interferents reactions (r_i)	k_{r_i} (cm^3 s^{-1}) or ΔH_{r_i} (eV)	Analyte reaction (r_A)	k_{rA} (cm^3 s^{-1}) or DH_{rA} (eV)	ICP-DRC-MS S/Bckg improvement factor [Reference]
10	Be	1.51×10^6	B	1.68×10^4	$B^+ + CF_4 \rightarrow BF^+ + CF_3$	0.72 eV	$Be^+ + CF_4 \rightarrow BeF^+ + CF_3$	−0.48 eV	
14	C	5730	N	8.39×10^4	$N^+ + H_2 \rightarrow NH^+ + H$	5×10^{-10} [27]	$C^+ + H_2 \rightarrow CH^+ + H$	1.2×10^{-16} [27]	
26	Al	7.17×10^5	Mg	6.04×10^3	$Mg^+ + SF_6 \rightarrow MgF^+ + SF_5$	−0.80 eV	$Al^+ + SF_6 \rightarrow AlF^+ + SF_5$	0.75 eV	
32	Si	150	S	1.54×10^4	$S^+ + NO \rightarrow NO^+ + S$	3.4×10^{-10} [27]	$Si^+ + NO \rightarrow$ no reaction	$<10^{-11}$ [27]	5×10^4 [present paper]
36	Cl	3.01×10^5	S	2.93×10^4	$S^+ + C_2H_2 \rightarrow CHCS^+ + H$	9.7×10^{-10} [27]	$Cl^+ + C_2H_2 \rightarrow$ no reaction	$<2.6 \times 10^{-11}$ [27]	
39	Ar	269	K	6.42×10^4	$K^+ + I_2 \rightarrow KI^+ + I$	1.39 eV	$Ar^+ + I_2 \rightarrow ArI^+ + I$	Observed [40]	
40	K	1.28×10^9	Ar Ca	2.84×10^4	$Ar^+ + N_2O \rightarrow$ products $Ca^+ + N_2O \rightarrow CaO^+ + N_2$	3.0×10^{-10} [27] 1.6×10^{-10} [28]	$K^+ + N_2O \rightarrow$ no reaction	$<10^{-13}$ [28]	1.9×10^3 [present paper] 50 [present paper]
41	Ca	1.03×10^5	K	9.06×10^4	$K^+ + N_2O \rightarrow$ no reaction $Fe^+ + N_2O \rightarrow FeO^+ + N_2$	$<10^{-13}$ [28] 3.7×10^{-11} [28]	$Ca^+ + N_2O \rightarrow CaO^+ + N_2$	1.6×10^{-10} [28]	
53	Mn	3.74×10^6	Cr	8.26×10^4	$Cr^+ + ClO_2 \rightarrow CrO^+ + ClO$	−0.71 eV	$Mn^+ + ClO_2 \rightarrow MnO^+ + ClO$	0.104 eV	
59	Ni	7.60×10^4	Co	5.12×10^4	$Co^+ + N_2O \rightarrow$ products	2.1×10^{-12} [28]	$Ni^+ + N_2O \rightarrow Ni{\cdot}N_2O^+$	6.5×10^{-13} [28]	6 [present paper]
60	Fe	1.5×10^6	Ni	1.8×10^4	$Ni^+ + N_2O \rightarrow Ni{\cdot}N_2O^+$	6.5×10^{-13} [28]	$Fe^+ + N_2O \rightarrow FeO^+ + N_2$	3.4×10^{-11} [28]	0.08 [present paper]
79	Se	2.8×10^5	Br	4.87×10^5	$Br^{+*} + O_2 \rightarrow O_2^+ + Br$	7.1×10^{-10} [50]	$Se^+ + O_2 \rightarrow$ no reaction	[36]	7.2×10^3 [present paper]
81	Kr	2.29×10^5	Br	2.68×10^5	$Br^+ + C_2H_2 \rightarrow C_2H_2^+ + Br$	8.9×10^{-10} [27]	$Kr^+ + C_2H_2 \rightarrow$ no reaction	$<10^{-12}$ [27]	1.5×10^4 [present paper]
87	Rb	4.75×10^{10}	Sr	2.87×10^5	$Sr^+ + N_2O \rightarrow SrO^+ + N_2$ $Sr^+ + CH_3F \rightarrow SrF^+ + CH_3$	6.3×10^{-11} [28] $\sim 1/6\, k_c$ [36]	$Rb^+ + N_2O \rightarrow$ no reaction $Rb^+ + CH_3F \rightarrow$ no reaction	$<10^{-13}$ [28] [24]	1.2×10^4 [13] 10^3 [24]
91	Nb	680	Zr	6.73×10^4	$Zr^+ + C_6F_6 \rightarrow ZrF_2^+, ZrF_3^+$	9.3×10^{-10} [54]	$Nb^+ + C_6F_6 \rightarrow NbF_4^+, NbF_3^+, Nb^+{\cdot}C_6F_6$	8.6×10^{-10} [54]	
92 94	Nb	3.47×10^7 2.03×10^4	Zr Mo	2.4×10^5	$Zr^+ + C_6F_6 \rightarrow ZrF_2^+, ZrF_3^+$ $Mo^+ + C_6F_6 \rightarrow Mo^+{\cdot}C_6F_6$	9.3×10^{-10} [54] 2.7×10^{-10} [54]	$Nb^+ + C_6F_6 \rightarrow NbF_4^+, NbF_3^+, Nb^+{\cdot}C_6F_6$	8.6×10^{-10} [54]	
93	Mo	4.00×10^3	Nb Zr	2.77×10^5	$Nb^+ + N_2O \rightarrow NbO^+, NbN^+$ $Zr^+ + N_2O \rightarrow ZrO^+ + N_2, ZrN^+$	6.5×10^{-10} [27] 7.7×10^{-10} [27]	$Mo^+ + N_2O \rightarrow Mo{\cdot}N_2O^+$	3.4×10^{-13} [27]	100 [present paper] 150 [present paper]
97	Tc	2.60×10^6	Mo	2.82×10^5	$Mo^+ + OCS \rightarrow MoS^+ + CO$	$\sim 1/4\, k_c$ [36]	$Tc^+ + OCS \rightarrow$?		
98	Tc	4.20×10^6	Mo Ru	5.42×10^4	$Mo^+ + OCS \rightarrow MoS^+ + CO$ $Ru^+ + OCS \rightarrow RuS^+ + CO$	$\sim 1/4\, k_c$ [36] $>1/2\, k_c$ [36]	$Tc^+ + OCS \rightarrow$?		
107	Pd	6.50×10^6	Ag	2.89×10^6	$Ag^+ + C_3H_8 \rightarrow$ no reaction	[27]	$Pd^+ + C_3H_8 \rightarrow PdC_2H_4^+, PdC_3H_6^+$	Proceeds [27]	
108	Ag	418	Pd	5.23×10^4	$Pd^+ + C_3H_8 \rightarrow PdC_2H_4^+, PdC_3H_6^+$	Proceeds [27]	$Ag^+ + C_3H_8 \rightarrow$ no reaction	[27]	
126	Sn	$\sim 1 \times 10^5$	Te Xe	2.90×10^4	$Te^+ + CH_4 \rightarrow TeCH_2^+, TeCH_4^+$	Proceeds [36]	$Sn^+ + CH_4 \rightarrow$ no reaction	[36]	
129	I	1.57×10^7	Xe	6.20×10^5	$Xe^+ + O_2 \rightarrow O_2^+ + Xe$	1.1×10^{-10} [27]	$I^+ + O_2 \rightarrow$ no reaction	[23,16]	>100 [16]
135	Cs	2.30×10^6	Ba	4.67×10^5	$Ba^+ + N_2O \rightarrow BaO^+ + N_2$	2.4×10^{-10} [28]	$Cs^+ + N_2O \rightarrow$ no reaction	$<10^{-13}$ [28]	8×10^4 [present paper]
137 138	La	6.00×10^4 1.05×10^{11}	Ba	2.06×10^5	$Ba^+ + O_2 \rightarrow$ no reaction	$<10^{-13}$ [51]	$La^+ + O_2 \rightarrow LaO^+ + O$	4.3×10^{-10} [30]	40 [present paper]
146	Sm	1.03×10^8	Nd	1.92×10^6	$Nd^+ + CO_2 \rightarrow NdO^+ + CO$	8.0×10^{-11} [27]	$Sm^+ + CO_2 \rightarrow Sm{\cdot}CO_2^+$	Observed [36]	1.5×10^5 [present paper]
150	Gd	1.79×10^6	Nd Sm	1.08×10^5	$Nd^+ + NO \rightarrow NdO^+ + N$ $Sm^+ + NO \rightarrow Sm{\cdot}NO^+$	$\sim 1/10\, k_c$ [36] $<1/10\, k_c$ [36]	$Gd^+ + NO \rightarrow GdO^+ + N$	$\sim 1/2\, k_c$ [36]	
154	Dy	3.00×10^6	Sm Gd	6.95×10^4	$Gd^+ + N_2O \rightarrow GdO^+ + N_2$ $Sm^+ + N_2O \rightarrow SmO^+ + N_2$	5.3×10^{-10} [28] 1.4×10^{-10} [28]	$Dy^+ + N_2O \rightarrow DyO^+ + N_2$	2.7×10^{-11} [28]	
166	Ho	1.20×10^3	Er	8.33×10^4	$Er^+ + CF_4 \rightarrow ErF^+ + CF_3$	0.061 eV	$Ho^+ + CF_4 \rightarrow HoF^+ + CF_3$	0.234 eV	
176	Lu	3.78×10^{10}	Hf Yb	1.53×10^6	$Hf^+ + NO \rightarrow HfO^+ + N$	−0.99 eV	$Lu^+ + NO \rightarrow LuO^+ + N$	0.75 eV	2.8×10^3 (Lu/Hf) [present paper]
187	Re	4.35×10^{10}	Os	6.23×10^7	$Os^+ + N_2O \rightarrow OsO^+ + N_2$	5.8×10^{-11} [28]	$Re^+ + N_2O \rightarrow ReO^+ + N_2$	$<10^{-13}$ [28]	2.8×10^4 [present paper]
190	Pt	6.50×10^{11}	Os	1.28×10^5	$Os^+ + OCS \rightarrow OsS^+ + CO$	$\sim 4/5\, k_c$ [36]	$Pt^+ + OCS \rightarrow PtO^+ + CS$	$\sim 4/5\, k_c$ [36]	
192	Ir	241	Os Pt	1.71×10^5	$Pt^+ + OCS \rightarrow PtO^+ + CS$	$\sim 4/5\, k_c$ [36]	$Ir^+ + OCS \rightarrow IrS^+ + CO$	$\sim 4/5\, k_c$ [36]	
194	Hg	444	Pt	7.04×10^4	$Pt^+ + CH_3F \rightarrow CHFPt^+ + H_2$	$\sim 9/10\, k_c$ [36]	$Hg^+ + CH_3F \rightarrow HgCH_3F^+$	$<1/10\, k_c$ [36]	
202	Pb	5.25×10^4	Hg	1.33×10^5	$Hg^+ + NH_3 \rightarrow NH_3^+ + Hg$	$\sim 1/2\, k_c$ [36]	$Pb^+ + NH_3 \rightarrow PbNH_3^+$	$<1/10\, k_c$ [36]	
242	Am	141	Pu	3.00×10^5	$Pu^+ + NO \rightarrow PuO^+ + N$	$0.17\, k_c$ [52]	$Am^+ + NO \rightarrow AmO^+ + N$	$<0.001\, k_c$ [53]	10^3 [25]

For ^{63}Ni/^{63}Cu, ^{93}Zr/^{93}Nb/^{93}Mo, ^{158}Tb/^{158}Gd/^{158}Dy, ^{163}Ho/^{163}Dy, ^{182}Hf/^{182}W, ^{205}Pb/^{205}Tl, ^{208}Bi/^{208}Pb, ^{209}Po/^{209}Bi, ^{236}U/^{236}Np, ^{242}Pu/^{242}Am and ^{247}Cm/^{247}Bk resolving chemistries were not found.

ICP-MS practitioners who develop new methods of detection of interfered analytes [17]. There are some caveats, however, in direct applicability of the ICP-SIFT rate constants data to measurements with the reaction cells used in commercial ICP-MS; these include kinetic and internal energy effects on reaction and capture rates [37,38,10], and the much lower probability of termolecular reactions at ≤0.05 Torr pressure used in the cell-based ICP-MS (compared to SIFT or DT usually operated at >0.3 Torr pressure) [27]. In the absence of kinetic data, selection of candidate reactions can be approached by considering the free energy of the proposed reactions, which in most cases can be approximated (due to the relatively small change of entropy in bimolecular reactions of atomic ions with relatively simple molecules) by the enthalpy of reaction which can be calculated from the heats of formation of the products and reactants [39,13]. Not all exothermic reactions proceed, however, and suitability of a particular neutral for isobar separation must be experimentally verified under conditions obtained in a particular ion–molecule reactor.

The present paper considers reactions that can potentially be used for resolving long-lived radio-isotopes ($100 < T_{1/2} < 10^{12}$ years) from their long-lived or stable ($T_{1/2} > 100$ years) atomic isobars (see Table 1). For the 35 isobaric overlaps listed, some of the suggested chemistries have been previously used in ICP-MS. In some cases, predictions of the outcome can be made based on the kinetic data available, while in other cases, only enthalpies of reactions can be evaluated and indicate potentially favourable difference in reactivity. New results for the most favourable separations of 14 atomic isobaric cations in reactions with NO, N_2O, O_2, CO_2, C_2H_2, carried out by ICP-DRC-MS are presented. For some of the interfered long-lived radio-isotopes with $T_{1/2} > 100$ years, no suitable reaction could be suggested due to a lack or insufficiency of kinetic and/or thermo-chemical data, thus the isobars ^{63}Ni/^{63}Cu, ^{93}Zr/^{93}Nb/^{93}Mo, ^{158}Tb/^{158}Gd/^{158}Dy, ^{163}Ho/^{163}Dy, ^{182}Hf/^{182}W, ^{205}Pb/^{205}Tl, ^{208}Bi/^{208}Pb, ^{209}Po/^{209}Bi, ^{236}U/^{236}Np, ^{242}Pu/^{242}Am and ^{247}Cm/^{247}Bk are not listed in Table 1.

In some cases, for relatively highly abundant isotopes, the separations demonstrated are sufficient to be of practical use by ICP-MS. One of the potential applications of such "chemical resolution" of isobars is in situ Laser Ablation ICP-MS, when chemical separation of overlapping isobars before ICP-MS analysis is impossible.

Some of the separations studied in this paper (for measurement of isobars that are extremely different in abundance) can be of interest mainly to accelerator mass spectrometry (AMS) [1], which handles the problem of isobar separation in very different ways. The molecular isobars are removed completely during acceleration in a tandem accelerator where they fall apart due to their higher degree of ionisation, after charge changing at the higher energies. Usually molecules with three or more electrons removed are too unstable and can be completely eliminated. This is not a trivial problem when isotope ratios of 10^{15} are to be analysed but it can be done [41,42]. Atomic isobars present a formidable problem, which can be solved in a variety of ways. In some cases, such as ^{14}N and ^{14}C, the use of negative ions solves the problem as the lifetime of the N^- ion is very short and it does not survive the mass spectrometry, unlike the stable $^{14}C^-$ ion. The abundant CH^- and $CH_2{}^-$ molecules are destroyed during the changing of the charge from negative to positive in the tandem accelerator as mentioned above. Unfortunately there are only four atomic cases where the instability of the negative ion helps the isobar separation. They are Al/Mg, I/Xe, Pb/Hg and, of course, C/N.

The atomic isobars can, however, be separated at higher energies after tandem acceleration to many MeV. This can be done by, for example, rate of energy loss, dE/dx, measurements on each ion, as the dE/dx is a function of the charge on the nucleus. This method can be used but becomes more and more difficult as the elements get heavier. Many schemes have been adopted for separating isobars but they all get better as the ion energy increases. As the cost of an accelerator mass spectrometer increases rapidly with ion energy, such devices tend to be tandem accelerators used also for nuclear physics research and indeed the first AMS machines were just that. The expense of operating such devices is huge compared to say an ICP-MS device so alternative methods for isobar separation before tandem acceleration have been under development for over a decade [43,44].

Ionic reactions at keV energy, at the ion sources of such large machines, can separate isobars but the scattering during electron transfer is prohibitive for all but those reactions with the largest cross sections [44,45]. Resonant electron transfer reactions are possible for such separations but they are limited in number and for negative ions the accompanying large destruction cross sections make them in general inefficient. It was for this reason that the early discoveries of reactions at eV energy were so attractive, especially after the invention of the scattering control, which followed the work of Douglas and French [5].

AMS, as it is practised at present, has the problem that negative ions are required for the acceleration in a tandem accelerator, which is suitable for the detection of ^{14}C, ^{26}Al, ^{129}I and ^{202}Pb. As the use of higher energy also allows other long-lived rare isotopes to be analysed, negative ions have dominated AMS. Tandem electrostatic accelerators are convenient to use and relatively cheap compared with other accelerators. However, most of the work with reaction cells has been done with cations, whereas anions are required for tandem accelerators. Actually tandem accelerators were used in 1960 for atoms that did not form negative ions such as neon and nitrogen and this was done for nuclear physics purposes by what was called neutral injection [46]. Such a technology is possible for the cations that follow reaction cells so that it is possible to adapt the isobar separation methods for cations to AMS using neutral injection. This has so far not been done.

It is also possible to make anions from cations after a reaction cell so that an alternative approach is possible, but this has not yet been tried. Some of the examples discussed in this paper could be applicable to either neutral injection methods or to anionic methods especially in the cases where molecular ions are created during isobar separation in a reaction cell. Molecules can often make anions more readily than the parent atomic cation. Ca^+ is an example. The Ca^- anion has a binding energy of only 23 meV and so is extremely fragile and hard to create. However,

Table 2
Instrument parameters (ELAN DRC^{Plus} ICP-MS)

Energy state	Normal	Low	High
Plasma power (W)	1100	600	1600
Plasma gas flow (L min^{-1})	15	15	15
Auxiliary gas flow (L min^{-1})	0.75	0.75	0.75
Nebulizer gas flow (L min^{-1})	1.04	1.04	1.04
Lens potential, V_{lens} (V)	Auto	4	6.5
DRC entrance lens, potential, V_{entr} (V)	−15	0	−25
Axial field potential, V_{AFT} (V)	250	0	350
DRC rods offset, V_{CRO} (V)	−2	0	−2.5
DRC exit lens potential, V_{exit} (V)	−15	0	−30
$RP_q = 1.05q$	0.45	0.15	0.65
$Rp_a = 0.53a$	0	0	0
Mass filter rods offset, QRO (V)	−7.5	−5.5	−8
Ion current (pA)	>10^3 (matrix)	<1	>10^3 (100 ppm Au)
Nebulizer	PFA-100 (ESI, Omaha Nebraska)		
Spray chamber	Quartz cyclonic		
Reaction gas	On	On	On

the CaO^+ or the CaF^+ ions created in a reaction cell can be readily converted to anions.

The ionic reactions discussed in this paper are therefore applicable to mass spectrometry in general and there is every indication that reaction cells will play their part for in situ isotope ratio measurements with low-energy mass spectrometers, as well as in the higher energy mass spectrometry known as AMS. The later has the added advantage of having essentially no dark current (flux) because of the higher ion energy.

For rare radio-isotopes the rarity implies the need for ion sources giving very large ion currents. For the isotope ratios of 10^{-12} and below the ion currents in excess of 16 μA (e.g., 10^{14} ions/s) are required in order to get reasonable statistical errors of the measurement. Such currents require keV ion energies to be reached quickly to reduce space charge effects. Consequently, the conventional ICP ion source with its space charge limitations is not ideal for a direct application to AMS. A high extraction field arrangement for extracting such high currents (∼200 μA) from an atmospheric pressure ICP has been developed [47], and it was suggested that it could potentially be used in AMS, providing a versatile method of ionisation for atoms with different ionisation potentials. For using ion-molecule reactions at ∼eV energies for such high current beams, mass separation of the rare isotopes from the abundant ones at keV energy is required, with consequent retardation and ion cooling. Such new and significant development is outside of the scope of this work, which is exploratory only. The separations discussed provide a starting point for their application to AMS.

2. Experimental

All measurements were performed with an ELAN DRC^{Plus} ICP-MS instrument (Perkin-Elmer SCIEX, Shelton CT) equipped with a dynamic reaction cell and two-channel gas manifold. The instrument has been described elsewhere [9,10,16]. Reaction gases O_2 (99.998%), N_2O (99.999%) (Matheson Gas Products, Whitby, Ontario, Canada), premixed 30% NO (99.96%) + 70% He (99.9995%) (Scott Specialty Gases) were introduced through an additional oxygen gas purifier (NuPure) while C_2H_2 (99.6%), CH_4 (99.999%), CH_3F (99%) (all Matheson Gas Products) were introduced via the purifier supplied with the instrument. As NO is unstable at high pressure, decomposing to N_2O and NO_2, additional purification of NO was needed and was enabled via a custom-made cold trap consisting of 20 feet × 1/4 feet i.d. stainless steel tubing wound into a spiral and submerged in either methanol/liquid nitrogen (melting point −98 °C) or ethanol-liquid nitrogen (−110 °C) slush. The parameters of the instruments were kept the same for all studied reactions and are given in Table 2 (column "Normal"), except for the experiments on the energy effects described below.

The effect of ion internal and translational energy on reactivity was studied by measuring reaction profiles in different "energy states" of the instrument. The instrument was modified to allow independent control of the entrance lens (V_{entr}), exit lens (V_{exit}) and the total ion current entering the cell (see Fig. 1). The "energy states" were defined by the plasma power (affects excitation and ionisation temperature and thus ion internal energy), ion lens potential (V_{lens}, defines kinetic energy band of ions transmitted into the DRC); potential on the entrance lens of the DRC (V_{entr}) and its rods offset (V_{CRO}) that define the kinetic energy to which ions are accelerated at the entrance; axial field strength defined by the potential applied to the axial field electrodes (V_{AFT}), parameters of ion in the radio-frequency quadrupolar field RPq and RPa (which approximate Mathieu parameters a and q) that influence ion translational energy in the rf field; potential on the exit lens of the cell (V_{exit}) which contributes to ion energy close to the cell exit, and the total ion current into the cell (which contributes to ion translational energy via coulombic repulsion). The energy effect on reactivity was studied using oxidation of Ba^+ and Eu^+ by O_2. Oxidation of Eu^+ is endothermic by 1.15 eV but was observed by ICP-SIFT and was attributed to the excited states produced in ICP [29]. Oxidation of Ba^+ is endothermic by the same 1.15 eV, and it has significantly (33%) populated in plasma at 5500 K two low

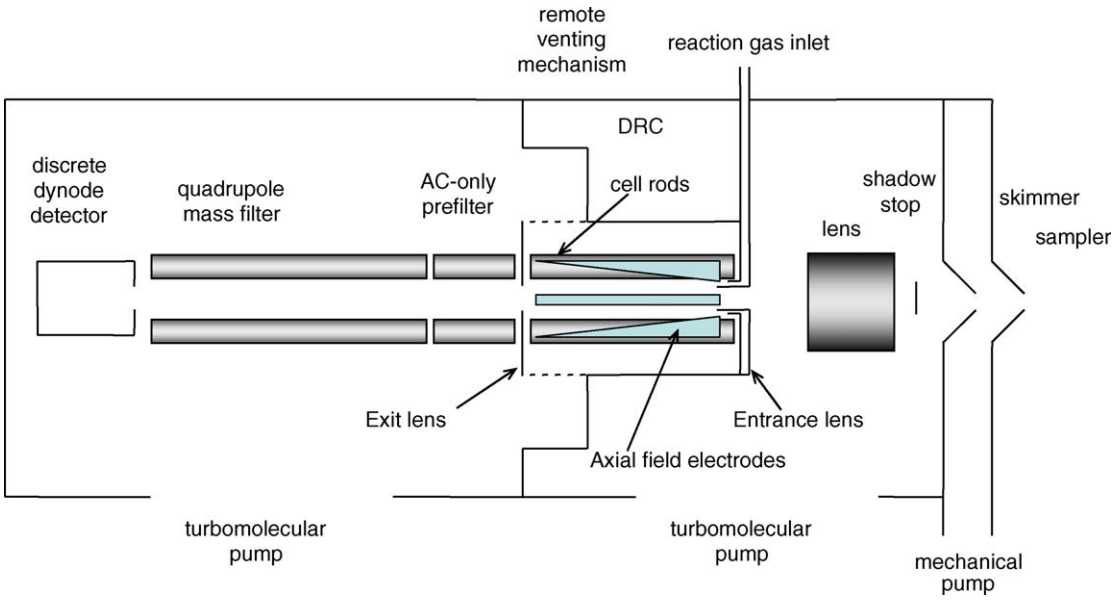

Fig. 1. Schematic diagram of the modified Elan DRC^{plus} ICP-MS. The details and the basics of operation of the instrument are described in [10,16,4].

lying ^{2}D states (0.6–0.7 eV) [30], which may exhibit different reactivity than the ground state.

Reactions of radio-isotopes in most cases were studied using stable isotopes, with the underlying assumption of similarity in reactivity. The kinetic isotope effect [48] can be significant for incomplete reactions (e.g., when an analyte ion is partially converted to product ion), and is of low significance when the interference is removed from the relatively non-reactive analyte or for complete reactions. 1000 μg mL^{-1} single element standards (Spex CertiPrep, Metuchen, USA) diluted with deionised water (DIW, ELIX/Gradient, Millipore, Bedford, MA) and HNO_3 or HCl (Baseline, Seastar Chemicals, Sidney, BC, Canada) were used for preparing samples of desired composition and concentrations. Reaction gas flows are specified in argon-equivalent standard cubic centimeter per minute (Ar-equiv. sccm), as set in the instrument software and controlled via Ar-calibrated mass flow controller. To obtain the true flow for a particular gas, the apparent value of the gas flow has to be multiplied by the correction coefficient (available from the MKS website [49]).

3. Results and discussion

3.1. Reactions with NO

The relatively low ionization potential of NO (9.264 eV) makes it an attractive candidate gas for charge-exchange removal of isobars with high ionization energy. The affinity of N to oxygen atom is relatively high (6.54 eV) and provides potential for good selectivity of oxygen-atom transfer to cations. Reaction rate constants for 46 atomic cations have been recently measured by ICP-SIFT [31]. Use of NO in ICP-DRC-MS for removing isobaric atomic interference of Pu^+ on Am^+, with three orders of magnitude increase of Am^+/Pu^+ ratio under optimum reaction gas flow and DRC conditions, was reported by Tanner et al. [25].

3.1.1. $^{32}Si^+/^{32}S^+$

Detection of $^{32}Si^+$ ($T_{1/2}$ = 172 a), used in dating of glacier ice [55], is interfered by isobaric $^{32}S^+$. Charge exchange of S^+ with NO is exothermic by 1.1 eV and proceeds relatively fast, while for Si^+ both charge-exchange and oxidation are endothermic by 1.1 and 1.55 eV, respectively, and are not observed (Table 1). Profiles of reactions of $^{28}Si^+$and $^{34}S^+$ with NO measured for single element standards at 1 and 12 mg/L in DIW, respectively, are shown in Fig. 2. Signals at m/z = 28 and 34 for the blank (DIW) reflect $^{14}N_2^+$ and $^{16}O^{18}O^+$ plasma matrix species. Charge exchange of N_2^+ and O_2^+ with NO is exothermic by 6.3 and 2.8 eV and are reported to proceed with rate constants evaluated at 4.6×10^{-10} and 4.1×10^{-10} cm^3 s^{-1}, respectively [27]. Slopes of decay measured with DRC reflect the reported similar high reactivity of S^+, N_2^+ and O_2^+ with NO and low reactivity of Si^+.

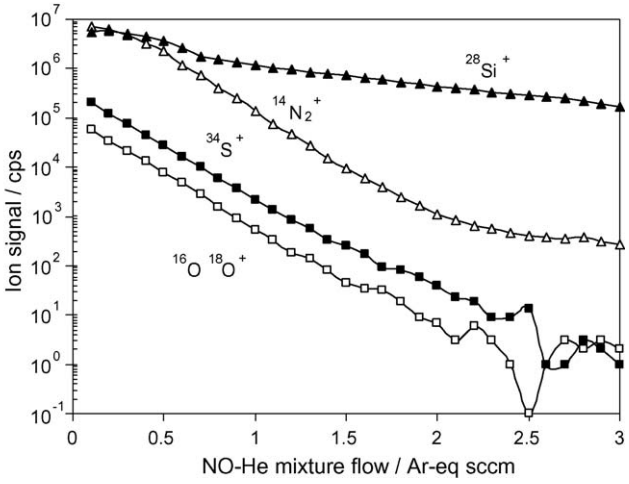

Fig. 2. Reaction profiles for Si^+, S^+, N_2^+ and O_2^+ with NO.

Incomplete decay of $^{14}N_2^+$ signal is attributed to the known fact that a significant amount of Si^+ is produced from the ICP torch (we observe a background equivalent concentration of approximately 1.4 μg/L, which suggests that NO may prove to be useful for detection of $^{28}Si^+$ in conventional ICP-DRC-MS applications, if a non-silicon containing injector is used). Analysis of net signals indicates an increase in the Si^+/S^+ ratio by a factor of approximately 5×10^4, which suggests that NO is a suitable gas for improving $^{32}Si^+$ detection in the presence of $^{32}S^+$. To be of interest for implementation in AMS, the extent of separation of 10^7 or higher needs to be shown (and is achieved in AMS by using negative ion injection of SiH_3^- which is much more abundant than SH_3^- [56]). Comparison of the slopes of decay for S^+ and Si^+ suggests that such separation can potentially be achievable at a flow above 4.5 Ar-equiv. sccm., at a cost of two orders of magnitude loss of Si^+. The loss of Si^+ is attributed to collisional scattering as well as to oxidation by impurities (more than two-fold decrease in SiO^+ formation was observed when the cold trap was operated at −110 °C compared to room temperature, not shown). Further purification of the reaction gas can potentially reduce the Si^+ loss. The molecular isobar O_2^+, which can be a problem for negative ion injection AMS since the anion is readily formed, is also removed at a similar or slightly higher rate compared to S^+. The newly formed by charge-exchange $^{14}N^{18}O^+$ and $^{15}N^{17}O^+$ molecular isobars are not a problem in the case of AMS since NO has very low electron affinity (0.026 eV) and thus will not be converted to negative ions efficiently, and because even if formed, the molecular isobars will be destroyed in the stripping canal anyway [1].

3.1.2. $^{176}Lu^+/^{176}Hf^+/^{176}Yb^+$

The lutetium–hafnium dating method requires quantitation of Hf and Lu isotopes including the overlapping ^{176}Hf and ^{176}Lu [57]. Since both are relatively abundant and the extent of separation does not need to be large, chemical resolution in a reaction cell may potentially be useful for in situ laser ablation analysis. Oxidation of Hf^+ by NO is exothermic by 0.99 eV, while oxidation of Lu^+ and Yb^+ is endothermic by 0.75 and 2.5 eV, respectively. Reaction profiles shown in Fig. 3 confirm the relatively fast oxidation of Hf^+ ($k_r = 5.6 \times 10^{-10}$ cm^3 s^{-1} [31]), while Lu^+ and Yb^+ signals increase due to collisional focusing in the pressurized quadrupole [5]. Unpublished data from the ICP-SIFT [36] show low reactivity of Lu^+ and Yb^+ towards NO.

Although Lu^+ loss was not observed, LuO^+ formation was significant despite the fact that the oxidation channel is endothermic. We attribute this to three potential causes: (1) incomplete purification of NO from N_2O, NO_2 and H_2O (confirmed by the observed dependence of LuO^+ and $LuOH^+$ formation on the cold trap temperature); (2) double-step oxidation e.g., $Lu^+ + NO + NO \rightarrow LuO^+ + N_2O$, similar to the process discussed by Blagojevic et al. [31]; (3) pumping of ion kinetic energies by rf heating in the quadrupole field operated at $q = 0.5$ (Mathieu parameter), which can lead to promotion of low endothermicity reactions [38]. Direct oxidation of Yb^+ is more endothermic, and YbO^+ formation is much slower. Potentially, the reaction can be useful at a low flow (∼0.5 Ar-equiv. sccm), when ^{176}Hf can be detected as $^{176}HfO^+$ at an improved ratio to the isobars (∼10×), and at a high flow, for detection of $^{176}Lu^+$ (for samples with low Yb content).

3.1.3. $^{81}Kr^+/^{81}Br^+$

^{81}Kr ($T_{1/2} = 2 \times 10^5$ a) is used in dating groundwater and polar ice [58]. Kr^+ is reported non-reactive with NO despite having an exothermic by 4.74 eV charge-exchange channel ($k_r < 1 \times 10^{-12}$ [59]). This fact is explained in [59] by a relatively large energy defect (0.2 eV) between the recombination energy of Kr^+ and the available excited states of the molecular ion NO^+, preventing resonance charge exchange, as well as by unfavourable Frank–Condon overlaps between the neutral molecule and the excited state molecular ion. Its isobar, $^{81}Br^+$, has exothermic by 2.55 eV charge-exchange channel and is reported to react, but at a low rate ($k_r = 4.1$–4.4×10^{-11} cm^3 s^{-1} [50,60]). We observed that Br^+ reaction proceeds slower than that of Ar_2^+ ($k_r = 4.4 \times 10^{-11}$ cm^3 s^{-1}[61]), giving no significant improvement in Kr^+/Br^+ ratio (see Fig. 4).

Better $^{81}Kr^+/^{81}Br^+$separation is achieved with acetylene as discussed in Section 3.4.1.

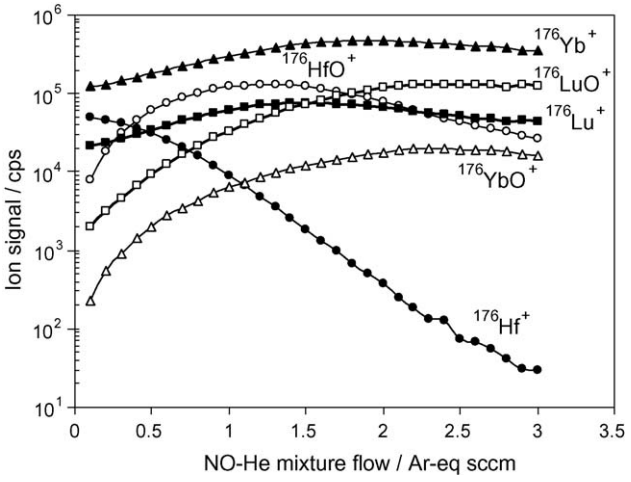

Fig. 3. Reaction profiles for Hf^+, Lu^+ and Yb^+ with NO.

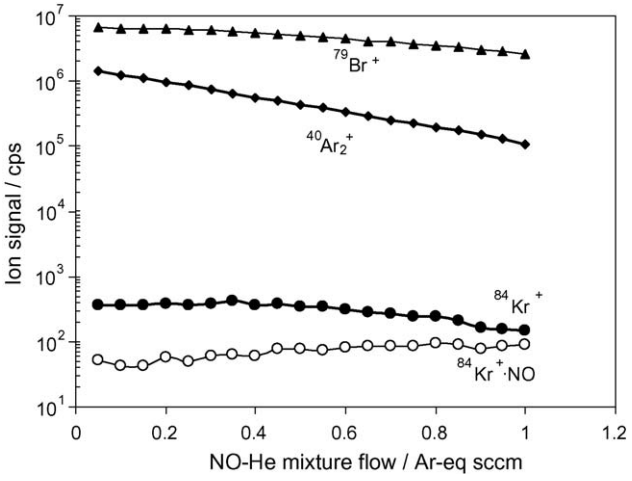

Fig. 4. Reaction profiles for Br^+, Kr^+ and Ar_2^+ with NO.

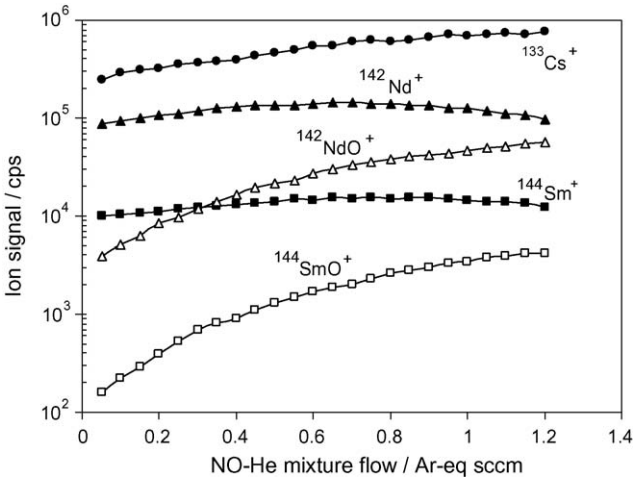

Fig. 5. Reaction profiles of Nd^+, Sm^+ and Cs^+ with NO.

3.1.4. $^{146}Sm^+/^{146}Nd^+$

^{146}Sm ($T_{1/2} = 1.03 \times 10^8$ a) is one of the extinct isotopes [62], which if found primordial, would be at $<10^{-17}$ fraction of Sm. If ^{146}Sm is recent supernova produced, in the interstellar grains it will be comparable in abundance to ^{146}Nd. Oxidation of Nd^+ is exothermic ($\Delta H_r = -1.33$ eV) while that of $^{146}Sm^+$ is endothermic (0.48 eV). Both Nd^+ and Sm^+ oxidise slowly at a similar rate (probably via two-step process $M^+ + NO + NO \rightarrow M^+{\cdot}ON + NO \rightarrow MO^+ + N_2O$, as reported by Bohme [63]), and no improvement in the Sm^+/Nd^+ ratio is observed (Fig. 5). Reaction profile of non-reactive Cs^+ is also given for comparison. Better $^{146}Sm^+/^{146}Nd^+$ separation is achieved with CO_2, as discussed in Section 3.4.2.

3.1.5. Potential for other separations with NO

^{93}Mo ($T_{1/2} = 3.5 \times 10^3$ a) which may be useful in exposure dating and needs to be detected at ultra-low level in nuclear waste [64] can potentially be resolved from ^{93}Nb and ^{93}Zr ($T_{1/2} = 1.5 \times 10^6$ a). Oxidation of Mo^+ by NO is endothermic by 1.61 eV and proceeds slowly via a two-step process ($k_r = 5.9 \times 10^{-12}$ cm^3 s^{-1} pseudo-bimolecular rate constant) whereas that of Nb^+ and Zr^+ is exothermic ($\Delta H_r = -2.46$ and -2.48 eV, respectively) and proceed at ~0.7 of capture rate ($k_r = 4.7 \times 10^{-10}$ cm^3 s^{-1} for both) [31].

$^{150}Gd^+$ ($T_{1/2} = 1.8 \times 10^6$ a) oxidation with NO is exothermic by 1.29 eV and has been shown to proceed at ~1/2 of the capture rate [36], while its stable isobars $^{150}Sm^+$ and $^{150}Nd^+$ oxidise slowly, as discussed above (see Fig. 5). The product ion $^{150}GdO^+$ can be detected at $m/z = 166$ at relatively low flows of NO (before significant oxidation of Sm^+ and Nd^+ occurs), although presence of major isotope ^{166}Er may hinder detection, since Er^+ is not oxidised with NO [36]. However, if mass selection is done before the ion-molecule reactor, Er^+ spectral overlap will be absent. Alternatively, after GdO and GdO^- creation and AMS, if dissociation of the GdO^+ product ions is enabled in the stripping canal, ^{150}Gd can be detected as the singly or multiply-charged atomic ion, while ^{166}Er will end up at a different m/z.

3.2. Reactions with N_2O

The N_2O ionization potential is 12.886 eV, which makes charge-exchange reactions endothermic for most atomic cations. The affinity of N_2 to oxygen atom is relatively low (1.735 eV), making oxidation exothermic for many cations. Reactivity of 60 atomic cations of metals have been systematically studied by ICP-SIFT [28,29]. In some cases nitration was reported to compete with oxidation. Spin conservation may play deciding role in exothermic oxidation reactions, since the ground states of N_2O and N_2 (the neutral product) are both singlets, thus a reactant cation and a product oxide ion must have the same spin. Use of N_2O in ICP-DRC-MS for resolving isobaric atomic overlap of Sr^+ and Rb^+ was reported [13].

3.2.1. $^{40}K^+/^{40}Ar^+/^{40}Ca^+$ and $^{41}Ca^+/^{41}K^+$

Detection of $^{40}K^+$ ($T_{1/2} = 1.28 \times 10^9$ a) is interfered by Ar^+ and Ca^+. It has been shown that the K^+/Ar^+ ratio can be improved by eight orders of magnitude in reactions with ammonia [11], however, Ca^+ is not suppressed. K^+ is non-reactive with N_2O ($k_r < 10^{-13}$ cm^3 s^{-1}), while Ar^+ and Ca^+ are reported to react ($k_r = 3 \times 10^{-10}$ cm^3 s^{-1} [27] and 1.6×10^{-10} cm^3 s^{-1} [28]), e.g., at ~0.3 and 0.17 of capture rate, respectively. Reaction profiles measured with ICP-DRC-MS (Fig. 6) show that K^+/Ar^+ can be improved by more than three orders of magnitude, while K^+/Ca^+ is enhanced by a factor of ~50. These improvement factors may be of interest for in situ analysis of interstellar grains. Recent super-nova material will be more enriched in 40 K than terrestrial material so such enhancement of K over Ca and Ar may be significant enough. The data also suggest that ^{41}Ca ($T_{1/2} = 1.03 \times 10^5$ a), an important radionuclide used in dating and neutron flux monitoring [81], can be separated from ^{41}K when measured as $^{41}CaO^+$ at $m/z = 57$. Oxidation of Ca^+ does not occur on every collision, however, about half of the ions are converted to the oxide at a flow of ~0.2 Ar-equiv. sccm, which should provide a significant improvement of CaO^+/KO^+ compared to Ca^+/K^+. The minor isotope $^{57}Fe^+$ (although somewhat suppressed, not shown) could potentially be a problem, how-

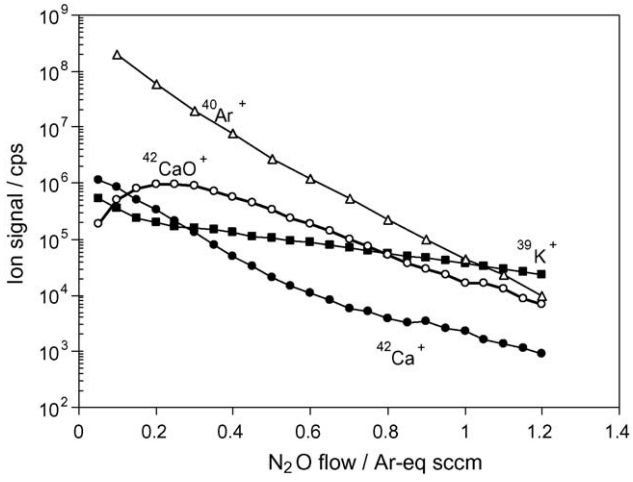

Fig. 6. Reaction profiles of $^{40}Ar^+$, $^{39}K^+$ and $^{42}Ca^+$ with N_2O. Initial faster decay of K^+ signal is due to reactive removal of $^{38}ArH^+$ isobaric plasma matrix ion.

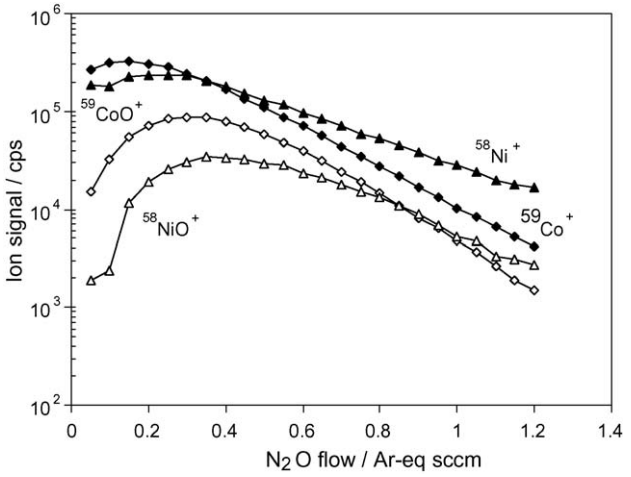

Fig. 7. Reaction profiles of Co^+ and Ni^+ with N_2O.

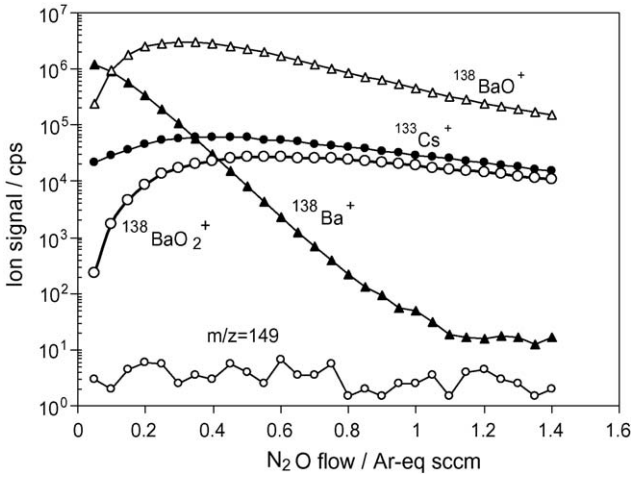

Fig. 8. Reaction profiles for Cs^+ and Ba^+ with N_2O.

ever, with mass pre-selection or neutral/anion stripping after the cell, as discussed above in Section 3.1.5 for ^{150}Gd, non-isobaric atomic interferences are not a problem for AMS. Further exploration of moving $^{41}Ca^+$ to molecular ion needs to include CaF^+ producing reactions, since it has very high electron affinity and thus its isobar-free generation may be of interest for negative ion injection AMS.

3.2.2. $^{59}Ni^+/^{59}Co^+$ and $^{60}Fe^+/^{60}Ni^+$

^{59}Ni ($T_{1/2} = 7.6 \times 10^4$ a) and ^{60}Fe ($T_{1/2} = 1.5 \times 10^6$ a) are cosmogenic isotopes used in meteorite exposure dating. Co^+ reacts with N_2O by oxidation and clustering faster than Ni^+ (which is reported to react by clustering only), at $k_r = 2.1 \times 10^{-12}$ and 6.5×10^{-13} $cm^3\ s^{-1}$ (pseudo-bimolecular rate for clustering), respectively [28]. Both cations have exothermic oxidation channels ($\Delta H_r = -1.11$ and -0.37 eV, respectively), although oxidation into a ground state oxide cation is spin forbidden [28]. We observed formation of NiO^+ and noticeable loss of Ni^+ (Fig. 7). It may be that rf-heating in the quadrupole operated at $q = 0.5$ contributes enough kinetic energy so that excited state oxide cations are formed in collisions, so that spin is conserved. The role of excited state of Ni^+ produced in plasma should be insignificant since its population is too low (calculated at 21% for 5500 K [28]) to explain Ni^+ loss. Co^+ removal is not fast, and improvement in Ni^+/Co^+ of only a factor of 6 is achieved in our ICP-DRC-MS experiment.

Fe^+ oxidation is faster than Ni^+ (3.7×10^{-11} $cm^3\ s^{-1}$) and could theoretically be used for detection of $^{60}FeO^+$. We observed, however, relatively fast further loss of FeO^+ (perhaps to clustering). As a result, there is no advantage in detecting Fe^+ as FeO^+ (in fact, FeO^+/NiO^+ ratio is an order of magnitude worse than the original Fe^+/Ni^+ ratio in the un-reacted beam). Other chemistries will have to be studied for separation of these isobars. One possibility is to use CH_3I which is reported to be reactive towards Fe^+, producing FeI^+, and less reactive towards Ni^+ and Co^+[65,66].

3.2.3. $^{135}Cs^+/^{135}Ba^+$

Fission product ^{135}Cs ($T_{1/2} = 2.3 \times 10^6$ a) is an important isotope present in nuclear waste and fall-out and also used as oceanic tracer. It is also suggested for ^{135}Cs–^{135}Ba chronometer [67] and for improving ^{137}Cs ($T_{1/2} = 30$ a) chronometer [68]. For detection by ICP-MS, the isobaric Ba can be removed via electrothermal vaporisation [69]. Cs^+ does not react with N_2O ($k_r < 10^{-13}$ $cm^3\ s^{-1}$) while oxidation of Ba^+ proceeds at 0.32 of capture rate ($k_r = 2.4 \times 10^{-10}$ $cm^3\ s^{-1}$) [28]. Reaction profiles obtained by ICP-DRC-MS [70] confirm that significant separation can be achieved. Neither loss of Cs^+ nor formation of CsO^+ and $Cs{\cdot}NO_2^+$ is observed, while Ba^+ is suppressed by almost five orders of magnitude (Fig. 8).

Further reaction of BaO^+ was observed to produce BaO_2^+ and $BaOH^+$ (probably from water impurities in the cell gas). Direct detection with ICP-DRC-MS can be somewhat complicated by formation of $^{119}SnO^+$ (Vivien Taylor, private communication 2004), however, this can be obviated if the ion–molecule reactor follows a first mass selection step, as discussed above for AMS. Mass spectra for $^{133}Cs^+$ measured with S/N > 100 in 500× excess of natural Ba by ICP-DRC-MS is shown in Fig. 9.

3.2.4. Re/Os

^{187}Re ($T_{1/2} = 4.35 \times 10^{10}$ a) is used in the ^{187}Re–^{187}Os geochronometer. Oxidation of both Os^+ and Re^+ with N_2O is exothermic ($\Delta H_r = -2.6$ and -3.25 eV, respectively), however, only Os^+ is reported to react at ~0.08 of the capture rate ($k_r = 5.8 \times 10^{-11}$ $cm^3\ s^{-1}$ and for $Re^+ < 10^{-13}$ $cm^3\ s^{-1}$, respec-

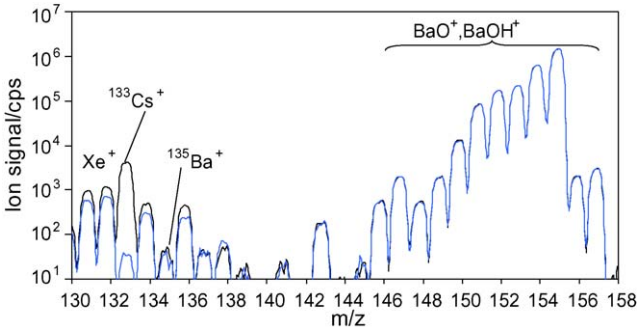

Fig. 9. Spectra for a blank (10 μg/L Ba) and a sample (10 μg/L Ba + 20 ng/L Cs) at $N_2O = 0.9$ Ar.-equiv. sccm.

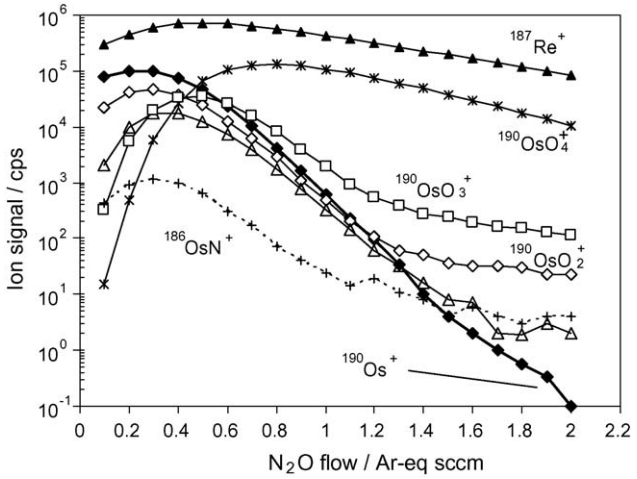

Fig. 10. Reaction profiles for Re^+ and Os^+ with N_2O.

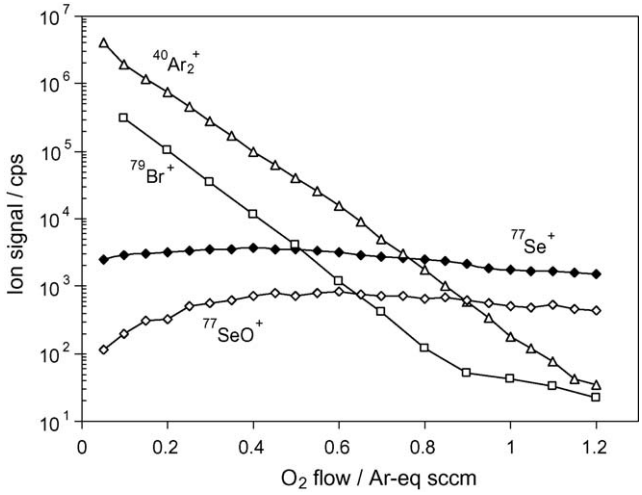

Fig. 11. Profiles of reactions of Br^+, Se^+ and Ar_2^+ with O_2.

tively) [28]. The failure of Re^+ to oxidise despite the significant exothermicity is attributed to the spin-forbidden transition between ground states of Re^+ and ReO^+ [28]. Reaction profiles measured with ICP-DRC-MS (Fig. 10) show that more than five orders of magnitude improvement of Re^+/Os^+ is achieved. Terminal product of Os^+ oxidation appears to be OsO_4^+, so one could think of simultaneous detection of Re and Os as OsO_4^+. Concurrent processes of N-atom transfer from N_2O and H-atom transfer (from gas impurities), however, make interpretation of the signal at +64 a.m.u impractical due to complexity of combination of isotopic abundances of ${}^nOs^mO_3{}^kN^+$, ${}^nOs^mO_3{}^kN^jH^+$, ${}^nOs^mO_4{}^+$ and ${}^nOs^mO_4{}^jH^+$ ($n = 184$, 186, 187, 188, 190, 192). This complication is not unlike the case of using CH_3F for removing Os^+ interference from Re^+: although Re^+/Os^+ ratio is improved by a factor of $\sim 3 \times 10^4$, a complicated combination of isotopes of Os, H and C prevents reliable interpretation of $OsCHF^+$ and higher Os-containing product ions [70].

In the cases when single $m/z = 187$ is pre-selected before the ion–molecule reactor, the ions at $m/z = 251$ will be products of ${}^{187}Os^+$. Conversion of Os^+ to high oxide cations can potentially be of interest for tandem AMS, since the OsO_3^+ and OsO_4^+ can be made readily into molecular anions.

3.3. Reactions with O_2

The ionization potential of O_2 is high enough (12.07 eV) to not provide exothermic oxidation channels for most of cations. O-atom affinity of O is 5.169 eV and provides potential for good selectivity of oxidation reactions. The potential of O_2 in ICP-MS for removing isobaric overlap of ${}^{129}Xe^+$ and ${}^{129}I^+$ via near-resonant charge exchange with Xe^+ has been reported [23,16].

3.3.1. $^{79}Se^+/^{79}Br^+$

Detection of ${}^{79}Se$ ($T_{1/2} = 2.8 \times 10^5$ a), a fission product present at substantial level in radioactive waste from the nuclear fuel cycle, is interfered by ${}^{79}Br$. Projectile X-ray detection after AMS separation improves ${}^{79}Se/{}^{79}Br$ ratio by about three orders of magnitude [71]. $Br^+({}^3P_2)$ charge-exchange with O_2 is endothermic by 0.22 eV, and the reaction is reported to proceed at room temperature only for the ${}^3P_1$ (0.39 eV) and ${}^3P_0$ (0.48 eV) excited states ($k_r = 1.6 \times 10^{-10}$ cm^3 s^{-1} [72] or 7.1×10^{-10} cm^3 s^{-1} [50]). Above 0.15 eV centre-of-mass energy (E_{CM}), the reaction is reported to proceed at the capture rate for the ground state [72]. Unpublished results available from [36] suggest that Se^+ is non-reactive. Se^+ is reported to form SeO^+ when reacted with O_2 in ICP-DRC-MS [73,74], and the reaction has been evaluated as exothermic by 24 kJ/mol (0.25 eV) [74]. Reactive loss of Se^+ is not significant and is compensated by collisional focusing (Fig. 11). Br^+ reacts slightly faster than Ar_2^+ (reported to react with $k_r = (0.72–1.2) \times 10^{-10}$ cm^3 s^{-1}, see [27] and references therein). It is not clear if the slower decay of $m/z = 79$ signal observed is due to ${}^{79}Br^+$ or to polyatomic ions formed in reactions with impurities (e.g., SeH^+). If the slower slope was attributed to quenching of excited states and/or scattering of the non-reacting ground state, the population of the excited states would have to be assumed at 99.95% which is unlikely (due to ~100 collisions with Ar during the continuum flow expansion through the sampler of the interface, so that at least some collisional quenching must occur). The kinetic energy with which Br^+ ions enter the cell under standard operating conditions ($E_{LAB} \sim 20$ eV hence $E_{CM} \sim 5.7$ eV) is large enough to keep E_{CM} above 0.15 eV for about seven collisions, thus potentially providing the necessary activation energy for the reaction of the $Br^+({}^3P_2)$ state. Although residual signal at $m/z = 79$ is above background (20–40 cps), the Se^+/Br^+ signal ratio is increased by a factor of 7000, with only 40% Se^+ lost compared to non-pressurised cell operation.

3.3.2. La^+/Ba^+

${}^{138}La$ ($T_{1/2} = 1.05 \times 10^{11}$ a) is used in ${}^{138}La$–${}^{138}Ce$ and ${}^{138}La$–${}^{138}Ba$ geochronometers. Detection of ${}^{138}La^+$ is interfered by highly abundant ${}^{138}Ba^+$, and a LaO^+ ion beam is used in TIMS instead [75]. ${}^{137}La^+$ ($T_{1/2} = 6.0 \times 10^4$ a) is interfered by ${}^{137}Ba^+$. Ba^+ oxidation by O_2 is endothermic by 1.15 eV and it is reported as non-reactive ($k_r < 10^{-13}$ cm^3 s^{-1} [51]). La^+ oxidises at 0.75 of the capture rate ($k_r = 4.3 \times 10^{-10}$ cm^3 s^{-1} [29]). ICP-

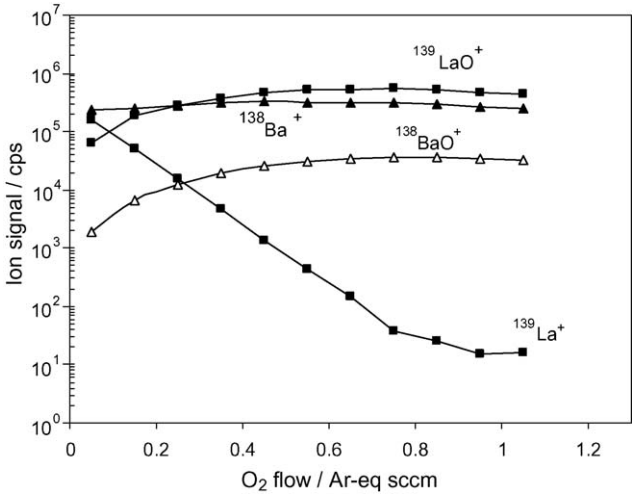

Fig. 12. Profiles of reactions of La^+ and Ba^+ with O_2.

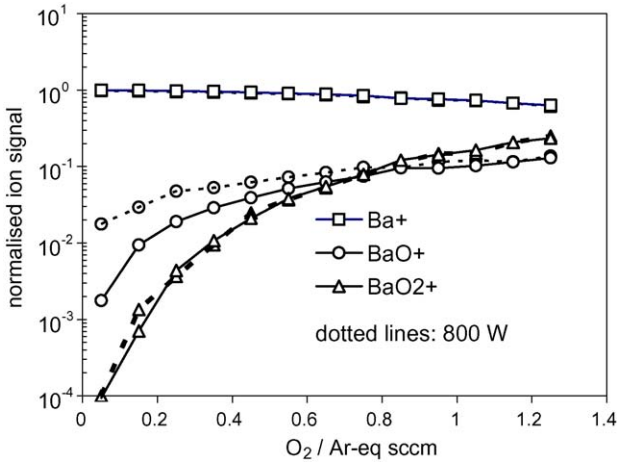

Fig. 13. Profiles of reaction of Ba^+ with O_2 at 1600 W (solid lines) and 800 W (dotted lines) ICP power in "low energy" state.

DRC-MS reaction profiles (Fig. 12) show high reactivity of La^+, but oxidation of up to 12% of Ba^+ is also observed at high O_2 flow. Detection of La as LaO^+ at a similar signal strength as for La^+ in the non-pressurised mode improves La^+/Ba^+ ratio by a factor of 40 (at O_2 flow of 0.15 Ar-equiv. sccm). The separation of $^{138}Ba^+$ from $^{138}La^+$ may be of interest for in situ studies of ^{138}Ba anomalies in early earth and meteorite samples.

Chemical resolution of ^{137}La from ^{137}Ba can be of interest for AMS exposure dating or fossil neutrino flux measurements. The attenuation of the Ba^+ must be very large in this case, so much higher extent chemical resolution will have to be developed.

The question of $^{138}Ce^+$ separation from $^{138}La^+$ arises when the chronometer is discussed. Ce^+ is oxidised by O_2 at a similar rate to La^+, thus different chemistries have to be considered.

3.3.2.1. Discussion of promotion of endothermic oxidation. The contribution of rf-field energy in the energetics of ion–molecule reactions is discussed in detail by Baranov et al. [10,38]. We have investigated how other parameters of the instrument affect promotion of oxidation and O_2-adduct formation of Ba^+ and Eu^+ (both endothermic by 1.15 eV) by changing one parameter at a time to their respective maxima from the "low energy" state of the system (see Section 2). Internal ion energy is a parameter that can potentially be varied by changing the power applied to the ICP. We did not observe any effect of changing power from 800 to 1600 W on oxide or adduct formation for Ba^+ (two ^2D states at 0.6 and 0.7 eV) or Eu^+ (^7S at 0.21 eV and five ^9D states at 1.23–1.38 eV). Profiles of reaction of Ba^+ with O_2 at 1600 and 800 W are shown in Fig. 13. At low flow, in-plasma produced BaO^+ dominates the oxide signal, and it is significantly lower for a hotter 1600 W plasma.

The effect of the "high energy state" on EuO^+ and EuO_2^+ formation in reactions with O_2 is shown in Fig. 14. Signal for Eu^+ is normalised on Cs^+ for accounting of scattering loss or collisional focussing (Cs^+ is not reactive, no CsO^+ or CsO_2^+ was observed).

Analysis of the effect of individual parameters showed the following. Acceleration of ions into the cell to $E_{LAB} = E_I + eV_{entr} = 31.5$ eV ($E_{cm} = 5.5$ eV) promotes oxidation at high O_2 flows, increasing $EuO^+/\Sigma_{n=0-2}(EuO_n)^+$ ratio from ~0.03 to 0.2 (at $O_2 = 1.2$ Ar-equiv. sccm), but has little effect at low and medium flows. Non-adiabatic conditions in the rf field, enabled at $q = 0.65$, promote oxidation, increasing $EuO^+/\Sigma_{n=0-2}(EuO_n)^+$ ratio from ~0.03 to ~0.08 for $O_2 > 0.3$ Ar-equiv. sccm. Acceleration of ions out of the cell by V_{exit}, the axial field strength and the space charge in the cell do not cause significant change in EuO^+ formation. EuO_2^+ formation is suppressed the most by the axial field ($EuO_2^+/\Sigma_{n=0-2}(EuO_n)^+$ changes from 0.2 to 0.002).

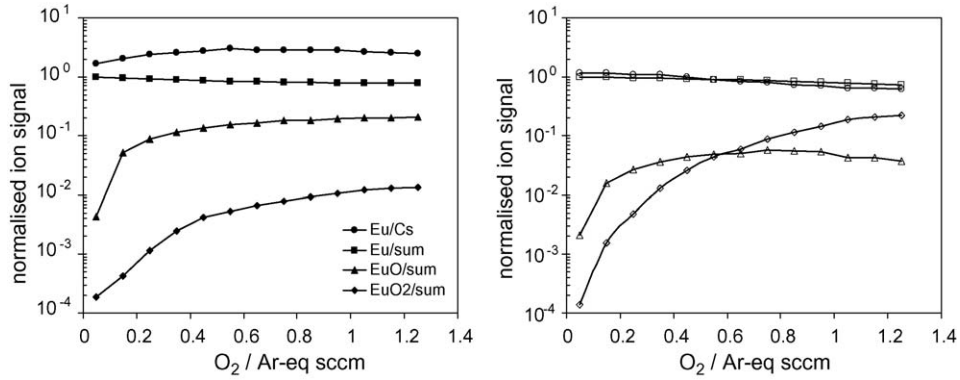

Fig. 14. Profiles of Eu^+ reaction with O_2 for "high energy state" (left) and "low energy state" (right). Sum = $Eu^+ + EuO^+ + EuO_2^+$.

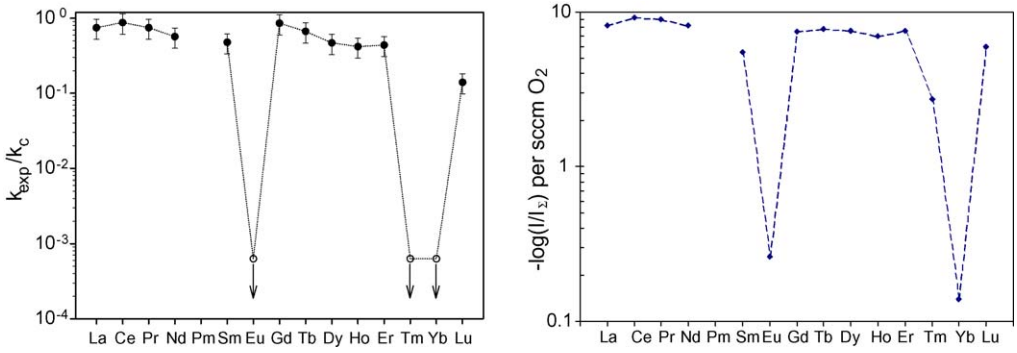

Fig. 15. Comparison of reaction efficiencies for $Ln^+ + O_2$ reactions measured with ICP-SIFT (data on left from [29], with permission) and with ICP-DRC-MS (expressed as $\log_{10}$ of ion signal suppression at 1 sccm of O_2).

It is also suppressed significantly by acceleration into the cell (from 0.2 to 0.02) and by the space-charge field (from 0.2 to 0.02), but only marginally by rf heating (from 0.2 to 0.1).

The effect of deviation of conditions from thermal is most observed for endothermic reactions. Exothermic reactions that are reported to proceed fast in the SIFT are similarly fast. The periodicity in lanthanide reactivity with O_2, for example, observed with ICP-DRC-MS, is similar to that for ICP-SIFT (see Fig. 15), although the relative difference in rates of fast and "non-proceeding" reactions is smaller.

The significant difference in reactivity of Tm^+ seen in Fig. 15, can be partially explained by a chart compilation error in [29], with the correct effective rate constant for Tm^+ being 0.003 (not 0.0006 as shown in the figure) (Greg Koyanagi, personal communication, 2005).

3.3.3. Re^+/Os^+ reactions with O_2

Neither Re^+ nor Os^+ form first oxides at a significant rate with O_2, consistent with the following relatively slow reactions reported with ICP-SIFT [30]:

$$Re^+ + O_2 \rightarrow ReO_2^+, \quad k_r/k_c \sim 0.0021 \tag{1}$$

$$Os^+ + O_2 \rightarrow OsO_2^+, \quad k_r/k_c \sim 0.00661 \tag{2}$$

$$ReO_2^+ + O_2 \rightarrow ReO_3^+ + O, \quad k_r/k_c \sim 0.111 \tag{3a}$$

$$ReO_2^+ + O_2 \rightarrow ReO_4^+ \tag{3b}$$

$$OsO_2^+ + O_2 \rightarrow OsO_4^+, \quad k_r/k_c \sim 0.0382, \tag{4}$$

with branching ratio for $k_{3a}/k_{3b} = 6{:}1$.

Formation of ReO_2^+ and OsO_2^+ is observed, and ReO_2^+ is further oxidised (mainly to ReO_3^+) faster than OsO_2^+ (which forms mainly OsO_4^+)(Fig. 16). Despite the absence of He buffer in the DRC, the reaction profiles show similar patterns to those reported for ICP-SIFT [30], despite the lower pressure in the DRC.

The dominant product ions at intermediate O_2 flow are OsO_2^+ and ReO_3^+, with signals somewhat stronger (due to collisional focussing) than the signals for bare atomic ions in the non-pressurised mode. This may allow simultaneous detection of Re^+ and Os^+ under one set of DRC conditions. Mass spectra for single element samples of Re and Os at 10 ng/mL (Fig. 17) show ~100-fold improvement of Os^+/Re^+ when $OsO_2^+$is measured, with 10-fold improvement of Re^+/Os^+ ratio when Re is detected as ReO_3^+.

The reactions 1–4 should probably be considered in view of the making of multiple oxides rather than a way to solve the Re–Os overlap, which was already discussed in Section 3.2.4. ReO_4 and OsO_3 have very high electron affinities, so the reaction-cell cations can potentially be made into very strong anions for negative ion injection AMS.

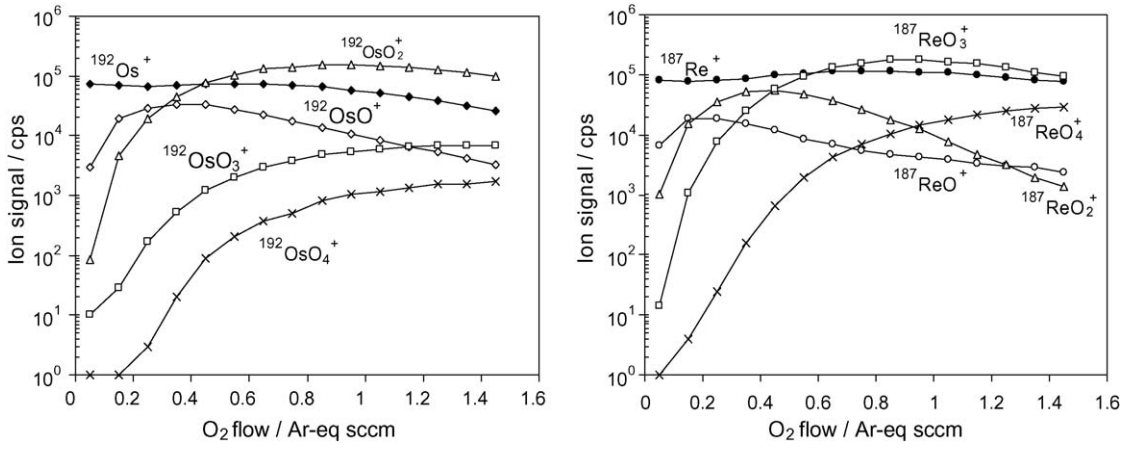

Fig. 16. Profiles of reaction of Os^+ and Re^+ with O_2.

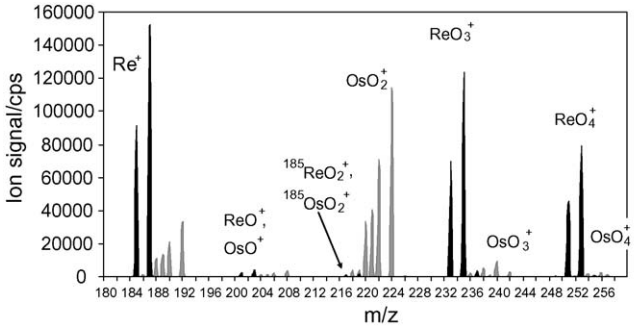

Fig. 17. Mass spectra for Re and Os samples measured at $O_2 = 1.5$ Ar-equiv. sccm and $q = 0.4$.

3.4. Reactions with other gases

3.4.1. Kr^+/Br^+ separation with C_2H_2

Charge exchange of Kr^+ and Br^+ with acetylene is exothermic for both, at $\Delta H_r = -2.6$ and -0.414 eV, respectively. Br^+ is reported to react at nearly the capture rate ($k_r = 8.9 \times 10^{-10}$ cm^3 s^{-1} [50]) while the more exothermic reaction for Kr^+ is reported as non-proceeding ($k_r < 10^{-12}$ cm^3 s^{-1} [76]). The latter fact was attributed to unfavourable Franck–Condon factors connecting C_2H_2 with the $C_2H_2^+$ [76] in highly vibrationally excited states at energy levels close to the recombination energy of the Kr^+. ICP-DRC-MS reaction profiles (Fig. 18) confirm the slow Kr^+ reaction (we attribute loss of Kr^+ to reactions with impurities in the 99.6% pure acetylene, e.g., H_2O and C_2H_4 that are both highly reactive with Kr^+).

The majority (>99%)of the Br^+ ions react very rapidly: the initial slope corresponds to $\times 10^4$ suppression of Br^+ per 0.1 sccm of C_2H_2 (we calculated the gas correction factor for C_2H_2 for the mass flow controller calibrated with Ar to be 0.42). There is a second slope in the reaction profile, which corresponds to $\times 10^9$ suppression per 1 sccm, and ~0.5% of Br^+ react at this slower rate. The dual slopes in the reaction profiles are usually explained by either the presence of other species (which is not the case since the $^{79}Br^+/^{81}Br^+$ isotope ratio is preserved throughout the profile), or the presence of excited states. Fast charge exchange of $Br^+(^3P_2)$ with C_2H_2, exothermic by 0.414 eV, is explained in [50] by the fact that the reaction can populate $C_2H_2^+$ ions in the low-lying vibrational levels of the ground ionic state with good Franck–Condon overlap with the acetylene molecule. The symmetrical C–H bond stretching mode of the $X\Sigma_u^+$ state of $C_2H_2^+$ (0.40097 eV) is almost at an exact energy coincidence with the reaction energy, which may explain its extremely high reaction rate. For $Br^+(^3P_1, ^3P_0)$ states, if they are present in the beam at a level of ~0.5%, more exothermic charge exchange (by 0.802 and 0.829 eV) requires higher vibrational levels of $C_2H_2^+$, not readily available [77]. The slow reacting $Br^+(^3P_{1,0})$ may be surviving excited states produced in the ICP and not quenched in the interface collisions with Ar. We attempted to influence their generation in the plasma by lowering the plasma power (and thus excitation and ionisation temperature) (Fig. 19).

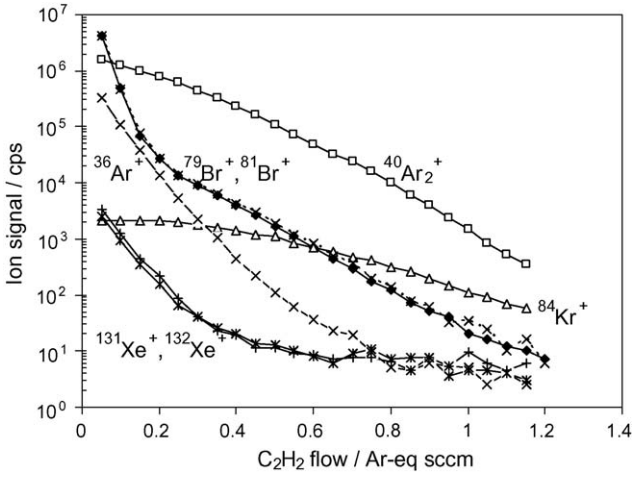

Fig. 18. Profiles of reactions of Br^+, Kr^+, Ar_2^+, Xe^+ and Ar^+ with C_2H_2.

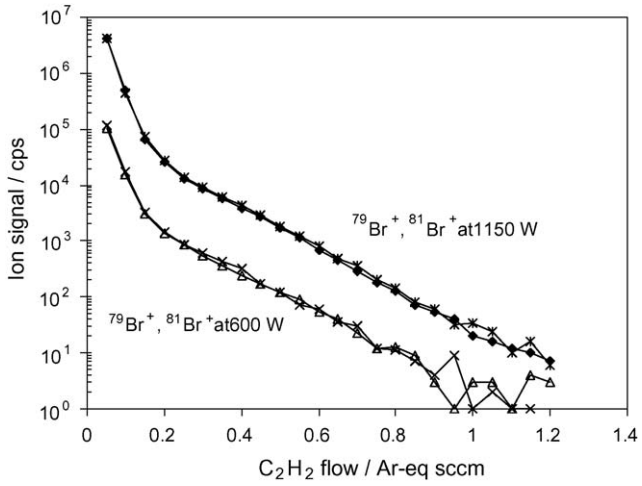

Fig. 19. Profiles of reactions of Br^+ with C_2H_2 at two different ICP power levels.

There was seemingly no effect on the dual rates difference or the inflection points, indicating that perhaps the excited states (on the level of 0.5%) are produced in the cell in energetic collisions at the entrance at up to $E_{CM} = 5.7$ eV (see Section 3.3.1), or due to ion heating in the rf field.

Nevertheless, although a fraction of Br^+ reacts slower, the overall gain in Kr^+/Br^+ signal ratio is improved by at least four orders of magnitude compared to the non-pressurised mode of operation. Better control of impurities to prevent Kr^+ loss and perhaps addition of a quenching gas before the reactor (for example, NO, as discussed in [72]), which potentially could assist full utilization of the fast reaction of Br^+, should allow achievement of even higher resolution.

3.4.2. Sm^+/Nd^+ separation with CO_2

Oxidation of both Nd^+ and Sm^+ with CO_2 is exothermic ($\Delta H_r = -2.35$ and -0.54 eV, respectively), however, unpublished results from SIFT [36] show that Sm^+ reacts only by CO_2-addition, while Nd^+ is oxidised at ~0.15 of the capture rate. The reaction rate for Nd^+ measured by FT-ICR is $k_r = 8.0 \times 10^{-11}$ cm^3 s^{-1} [78]. We observed relatively fast oxidation of Nd^+, with the Sm^+/Nd^+ ratio enhanced by a factor of more than 10^4 at $CO_2 = 1.4$ Ar-equiv. sccm (Fig. 20). The rela-

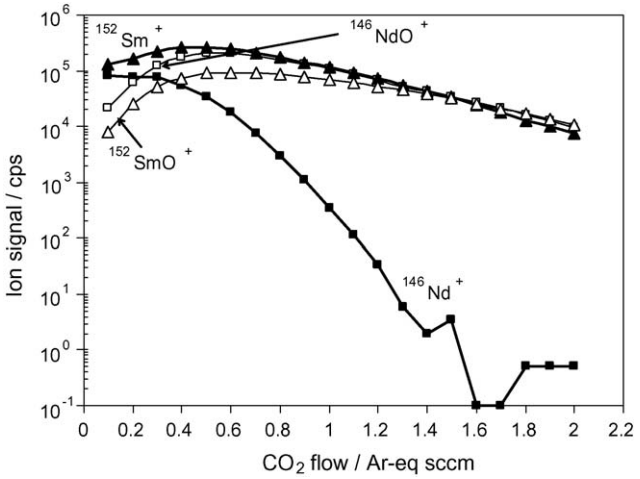

Fig. 20. Profiles of Sm^+ and Nd^+ reactions with CO_2.

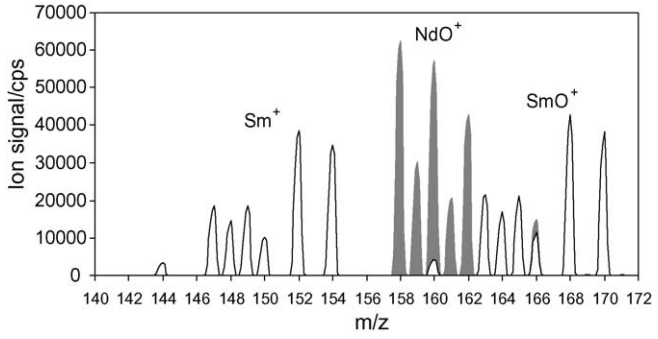

Fig. 21. Mass spectra for 10 ng/mL single element standards of Nd^+ and Sm^+ measured at $CO_2 = 1.4$ sccm and $q = 0.5$.

tively low reactivity of Sm^+ limits its loss to a modest two-fold. The mass spectra for 10 ng/mL single element standards of natural Nd and Sm show possibility of interference-free detection of $^{146}Sm^+$ in the presence of $^{146}Nd^+$ (Fig. 21).

3.4.3. Suggested reactions for atomic isobars separation

Potential ion–molecule chemistries for the remaining atomic isobars separation, for which either reaction rate constants or the reaction energetics could be found, are shown in Table 1. Perhaps the most interesting is the potential of separating $^{39}Ar^+$ ($T_{1/2} = 269$ a) by producing ArI^+ in reaction with I_2 vapour, with which K^+ reaction is endothermic by 1.39 eV. The intriguing fact that ArI^+ was observed [40] despite the existence of the highly exothermic (by 6.45 eV) charge exchange channel needs to be further explored.

4. Conclusions

Ion–molecule reactions at low eV energies enabled in the reaction cell show a remarkable ability to separate atomic isobars such as $^{40}Ar^+$ and $^{40}Ca^+$ and many others. In addition to the reduction of atomic isobars the reaction cell can reduce the unwanted molecular isobars, such as the $^{16}O_2{}^+$ molecular ion in the gas NO when studying the rare $^{32}Si^+$. The ion–molecule reaction cell therefore may rival AMS in the ability to attenuate isobars in many cases, in particular for moderate abundance ratios.

It can be expected that reaction cells incorporated into an AMS system may become more and more important since it makes resolution of the heaviest atomic isobars possible. The rate of energy loss difference between heavy isobars becomes smaller as the nuclear charge increases, making energy loss method used in AMS currently, less efficient for heavy elements. For the reaction cell, operation is dependent on the nuclear charge difference in the sense that the ion chemistry changes for each unit change in nuclear charge.

The complete elimination of ^{14}N and the molecules $^{12}CH_2$ and ^{13}CH by using anions and higher ion energy is unique to AMS. This has made possible the measurement of isotope ratios as small as 10^{-18} for $^{14}C/C$ [79]. Unfortunately the complete separation, by the instability of atomic anions, is limited to about four pairs in the whole periodic table. This is unlike chemical resolution, where it seems to be possible to find suitable reactions for a significant separation of most pairs of atomic ions studied so far.

The use of higher ion energy, which is usually over ~1 MeV, in AMS confers an additional advantage that the use of eV ion energies in reaction cells lacks. That is the almost complete disappearance of dark current or flux. This is because the ionisation detector measures pulses that are well above the electronic noise. In addition the pulses can also be used, at least for the lighter elements, to provide dE/dx information as well as an energy resolution approaching 1%.

The combination of the two techniques would seem to be ideal except for one problem and that is AMS almost always requires negative ions for acceleration in a tandem. Most reaction cell studies have used cations instead and so they would have to be converted into anions for most AMS applications. This is quite possible and here the great flexibility of the reaction cell can help by, for example, converting a cation such as Ca^+ into a molecular ion such as CaF^+, which has a much higher electron affinity after neutralisation at keV energies. The exploitation of anions in reaction cells is also possible [80] and it is expected that research and development for both cations and anions in reaction cells will continue and be applied to isobar separation problems in mass spectrometry and AMS.

Acknowledgements

Part of this work was carried by D.R.B., V.I.B. and S.D.T while working for MDS SCIEX, for which opportunity we are grateful. A.E.L. acknowledges the support of NSERC and the University of Toronto, during this work.

References

[1] A.E. Litherland, Ann. Rev. Nucl. Part. Sci. 30 (1980) 437;
see also C. Tuniz, J.R. Bird, D. Fink, G.F. Herzog, Accelerator Mass Spectrometry, CRC Press, Boca Raton, FL, 1998;
W. Kutchera, Int. J. Mass Spectrom. 242 (2005) 145.

[2] D.J. Douglas, Can. J. Spectrosc. 34 (1989) 38.
[3] J.T. Rowan, R.S. Houk, Appl. Spectrosc. 43 (1989) 976.
[4] S.D. Tanner, V.I. Baranov, D.R. Bandura, Spectrochim. Acta 57B (2002) 1361.
[5] D.J. Douglas, J.B. French, J. Am. Soc. Mass Spectrom. 3 (1992) 398.
[6] N. Yamada, J. Takahashi, K. Sakata, J. Anal. Atom. Spectrom. 17 (2002) 1213.
[7] I. Feldmann, N. Jakubowski, D. Stuewer, Fresenius J. Anal. Chem. 365 (1999) 415.
[8] M. Niemelä, P. Perämäki, H. Kola, J. Piispanen, Anal. Chim. Acta 493 (2003) 3.
[9] S.D. Tanner, V.I. Baranov, Atom. Spectrosc. 20 (1999) 45.
[10] V.I. Baranov, S.D. Tanner, J. Anal. Atom. Spectrom. 14 (1999) 1133.
[11] S.D. Tanner, V.I. Baranov, U. Vollkopf, J. Anal. Atom. Spectrom. 15 (2000) 1261.
[12] S.D. Tanner, V.I. Baranov, J. Am. Soc. Mass Spectrom. 10 (1999) 1083.
[13] D.R. Bandura, V.I. Baranov, S.D. Tanner, Fresenius J. Anal. Chem. 370 (2001) 454.
[14] C. Hagg, I. Szabo, Int. J. Mass Spectrom. Ion Processes 73 (1986), 237, 277.
[15] B.A. Thomson, C.L. Jollife. Spectrometer with Axial Field. US Patent 5,847,386 (December 8,1998).
[16] D.R. Bandura, V.I. Baranov, S.D. Tanner, J. Am. Soc. Mass Spectrom. 13 (2002) 1176.
[17] J.W. Olesik, D.R. Jones, J. Anal. At. Spectrom. 21 (2006) 141.
[18] J. Takahashi, N. Yamada, Bunseki Kagaku 53 (2004) 1257.
[19] N. Jakubowski, L. Moens, F. Vanhaecke, Spectrochim. Acta 53B (1998) 1739.
[20] M. Hamester, D. Wiederin, J. Wills, W. Kerl, C.B. Douthitt, Fresenius J. Anal. Chem. 364 (1999) 495.
[21] A.G. Marshall, C.L. Hendrickson, Int. J. Mass Spectrom. 215 (1–3) (2002) 59.
[22] A. Makarov, Anal. Chem. 72 (2000) 1156.
[23] G.C. Eiden, C.J. Barinaga, D.W. Koppenaal, Rapid Commun. Mass Spectrom. 11 (1997) 37.
[24] L.J. Moens, F.F. Vanhaecke, D.R. Bandura, V.I. Baranov, S.D. Tanner, J. Anal. Atom. Spectrom. 16 (2001) 991.
[25] S.D. Tanner, C.S. Li, V. Vais, V.I. Baranov, D.R. Bandura, Anal. Chem. 76 (2004) 3042.
[26] E.R. Gonzales, S.R. Garcia, C. Mahan, W. Hang, J. Radioanal. Nucl. Chem. 263 (2005) 457.
[27] V.G. Anicich, An index of the literature for bimolecular gas phase cation–molecule reaction kinetics, NASA/Jet Propulsion Laboratory, Report #03-19, 2003.
[28] V.V. Lavrov, V. Blagojevic, G.K. Koyanagi, G. Orlova, D.K. Bohme, J. Phys. Chem. A 108 (2004) 5610.
[29] G.K. Koyanagi, D.K. Bohme, J. Phys. Chem. A 105 (2001) 8964.
[30] G.K. Koyanagi, D. Caraiman, V. Blagojevic, D.K. Bohme, J. Phys. Chem. A 106 (2002) 4581.
[31] V. Blagojevic, E. Flaim, M.J.Y. Jarvis, G.K. Koyanagi, D.K. Bohme, J. Phys. Chem. A 109 (2005) 11224.
[32] G.K. Koyanagi, D.K. Bohme, J. Phys. Chem. A 110 (2006) 1232.
[33] G.K. Koyanagi, X. Zhao, V. Blagojevic, M.J.Y. Jarvis, D.K. Bohme, Int. J. Mass Spectrom. 241 (2005) 189.
[34] G.K. Koyanagi, V.V. Lavrov, V. Baranov, D. Bandura, S. Tanner, J.W. McLaren, D.K. Bohme, Int. J. Mass Spectrom. 194 (2000) L1.
[35] G.K. Koyanagi, V.I. Baranov, S.D. Tanner, D.K. Bohme, J. Anal. Atom. Spectrom. 15 (2000) 1207.
[36] http://www.chem.yorku.ca/profs/bohme/research/research.html.
[37] P.B. Armentrout, Int. J. Mass Spectrom. 200 (2000) 219.
[38] V.I. Baranov, D.R. Bandura, S.D. Tanner, Int. J. Mass Spectrom. 247 (2005) 40.
[39] S.G. Lias, J.E. Bartmess, J.F. Liebman, J.L. Holmes, R.D. Levin, W.G. Mallard, J Phys. Chem. Ref. Data 17 (Suppl. 1) (1988) 1 (also see http://webbook.nist.gov/chemistry/.
[40] A. Henglein, G.A. Muccini, Z. Naturforsch. 15A (1960) 584.
[41] M.-J. Nadeau, H.W. Lee, A.E. Litherland, K.H. Purser, X.-L. Zhao, Nucl. Instrum. Meth. B 223–224 (2004) 328.
[42] R.P. Beukens, H.E. Gove, A.E. Litherland, W.E. Kieser, X.-L. Zhao, Nucl. Instrum. Meth. B 223–224 (2004) 333.
[43] A.E. Litherland, Nucl. Instrum. Meth. B 92 (1994) 207.
[44] J.P. Doupé, A.E. Litherland, I. Tomski, X.-L. Zhao, Nucl. Instrum. Meth. B 223–224 (2004) 323.
[45] A.E. Litherland, I. Tomski, J.D. Doupé, Nucl. Instrum. Meth. B 204 (2003) 720.
[46] A.E. Litherland, L.R. Kilius, Nucl. Instrrum. Meth. B 123 (1997) 18.
[47] S. Al Moussalami, W. Chen, B.A. Collings, D.J. Douglas, Rev. Sci. Instrum. 73 (2002) 884.
[48] G.K. Koyanagi, D.K. Bohme, in: S. Nelms (Ed.), ICP Mass Spectrometry Handbook, Blackwell Publishing, Oxford, 2005, p. 336.
[49] http://www.mksinst.com/GasConversionTable.html.
[50] C.A. Mayhew, D. Smith, Int. J. Mass Spectrom. Ion Process. 100 (1990) 737.
[51] R. Johnsen, H.L. Brown, M.A. Biondi, J. Chem. Phys. 55 (1971) 186.
[52] M. Santos, J. Marcalo, A.P. de Matos, J.K. Gibson, R.G. Haire, J. Phys. Chem. A 106 (2002) 7190.
[53] M. Santos, J. Marcalo, J.P. Leal, A.P. de Matos, J.K. Gibson, R.G. Haire, Int. J. Mass Spectrom. 228 (2003) 457.
[54] D. Caraiman, G.K. Koyanagi, D.K. Bohme, J. Phys. Chem. A 108 (2004) 978.
[55] U. Morgenstern, L.K. Fifield, A. Zondervan, Nucl. Instrum. Meth. B 172 (2000) 605.
[56] J. Heinemeier, P. Hornshoj, H.L. Nielsen, N. Rud, M.S. Thomsen, Nucl. Instrum. Meth. B 29 (1987) 110.
[57] C. Münker, S. Weyer, E. Scherer, K. Mezger, Geochem. Geophys. Geosyst. 2 (2001) GC000183 (accessed online at http://www.earthref.org/cgi-bin/).
[58] B.E. Lehmann, H. Oeschger, H.H. Loosli, G.S. Hurst, S.L. Allman, C.H. Chen, S.D. Kramer, M.G. Payne, R.C. Phillis, R.D. Willis, N. Thonnard, J. Geophys. Res. 90 (1985) 1547.
[59] J.B. Laudenslager, W.T. Huntress Jr., M.T. Bowers, J. Chem. Phys. 61 (1974) 4600.
[60] M. Hamdan, N.W. Copp, K. Birkinshaw, N.D. Twiddy, J. Phys. B: Atom. Mol. Phys. 17 (1984) 849.
[61] R.J. Shul, B.L. Upschulte, R. Passarella, R.G. Keesee, A.W. Castleman Jr., J. Phys. Chem. 91 (1987) 2556.
[62] A. Prinzhofer, D.A. Papanastassiou, G.J. Wasserburg, Astrophys. J. 344 (1989) L81.
[63] D.K. Bohme, Proceedings of the 51st ASMS Conference on Mass Spectrometry Allied Topics, Montreal, Quebec, Canada, June 8–12, 2003.
[64] H. Artigalas, J.L. Debrun, L. Kilius, X.L. Zhao, A.E. Litherland, J.L. Pinault, C. Fouillac, C.J. Maggiore, Nucl. Instrum. Meth. B 92 (1994) 227.
[65] E.R. Fisher, L.S. Sunderlin, P.B. Armentrout, J. Phys. Chem. 93 (1989) 7375.
[66] E.R. Fisher, R.H. Schultz, P.B. Armentrout, J. Phys. Chem. 93 (1989) 7382.
[67] H. Hidaka, Y. Ohta, S. Yoneda, J.R. DeLaeter, Earth Planet. Sci. Lett. 193 (2001) 459.
[68] T. Lee, T.L. Ku, H.L. Lu, J.C. Chen, Geochim. Cosmochim. Acta. 57 (1993) 3493.
[69] M. Song, T.U. Probst, N.G. Berryma, Fresenius J. Anal. Chem. 370 (2001) 744.
[70] D.R. Bandura, V.I. Baranov, A.E. Litherland, S.D. Tanner, Proceedings of the 30th Meeting of Fed. An. Chem. Spectrosc. Soc. (FACSS), Ft. Lauderdale, October, 2003.
[71] M. He, S. Jiang, S. Jiang, L. Diao, S. Wu, C. Li, Nucl. Instrum. Meth. B 194 (2002) 393.
[72] M. Hamdan, N.W. Copp, K. Birkinshaw, N.D. Twiddy, J. Phys. B: Atom. Mol. Opt. Phys. 17 (1984) 849.
[73] D.R. Bandura, S.D. Tanner, V.I. Baranov, G.K. Koyanagi, V.V. Lavrov, D.K. Bohme, in: G. Holland, S.D. Tanner (Eds.), Plasma Source Mass Spectrometry: The New Millenium, The Royal Society of Chemistry, Cambridge, 2001, p. 130.

[74] B. Hattendorf, D. Gunter, Spectrochim. Acta. 58B (2003) 1.
[75] J.R. de Laeter, N. Bukilic, Int. J. Mass Spectrom. 244 (2005) 91.
[76] K. Giles, N.G. Adams, D. Smith, J. Phys. B: Atom. Mol. Opt. Phys. 22 (1989) 873.
[77] NIST Chemistry WebBook. NIST Standard Reference Database Number 69, June 2005 Release, http://webbook.nist.gov/chemistry/.
[78] H.H. Cornehl, R. Wesendrup, M. Diefenbach, H. Schwarz, Chem. Eur. J. 3 (1997) 1083.
[79] A.E. Litherland, H.E. Gove, R.P. Beukens, in: B. Cleveland, R. Ford, M. Chen (Eds.), Topical Workshop on Low radioactivity Techniques, American Institute of Physics CP 785, 2005, pp. 48–56.
[80] A.E. Litherland, I. Tomski, X.-L. Zhao, L.M. Cousins, J.P. Doupé, G. Javahery, W. E. Kieser, "Isobar separation at low energy for AMS", Nucl. Instrum. Meth. B, in press.
[81] D. Fink, R. Middleton, J. Klein, P. Sharma, Nucl. Instrum. Meth. B 47 (1990) 79.